Large-scale ozone episodes in Europe: Results from reanalysis and Earth System projections

Rodrigo Crespo-Miguel[a,*], Carlos Ordóñez[a], Ricardo García-Herrera[a,b], Jordan L. Schnell[c,d], Steven T. Turnock[e,f]

[a] Departamento de Física de la Tierra y Astrofísica, Facultad de Ciencias Físicas, Universidad Complutense de Madrid, Madrid, Spain

[b] Instituto de Geociencias (IGEO), Consejo Superior de Investigaciones Científicas–Universidad Complutense de Madrid (CSIC–UCM), Madrid, Spain

[c] Cooperative Institute for Research in Environmental Sciences, University of Colorado, Boulder, CO, United States of America

[d] NOAA Global Systems Laboratory, Boulder, CO, United States of America

[e] Met Office Hadley Centre, Exeter, United Kingdom

[f] University of Leeds, Met Office Strategic (LUMOS) Research Group, University of Leeds, Leeds, United Kingdom

Keywords

Surface ozone; air pollution; air quality; climate change; extreme events

* Corresponding author.
E-mail addresses: rodcresp@ucm.es (R. Crespo-Miguel), carlordo@ucm.es (C. Ordóñez), rgarciah@ucm.es (R. García-Herrera), jordan.schnell@noaa.gov (J. L. Schnell), steven.turnock@metoffice.gov.uk (S. T. Turnock)

Highlights

- A new algorithm for the identification of large-scale ozone episodes is presented.
- Largest episodes located in northern (southern-central) Europe in Apr-May (Jun-Sep).
- Large ozone episodes decreased from 2003 to 2022 in the CAMS reanalysis.
- Diverging changes in the sizes of ozone episodes in future projections.
- Emissions and climate change will determine the areal extent of future episodes.

Abstract

Episodes of high near-surface ozone concentrations tend to cover large areas for several days and are detrimental to human health and vegetation. They are strongly dependent on both meteorology and precursor emissions. This study introduces a new pseudo-Lagrangian algorithm that identifies the spatiotemporal patterns of episodes, allowing for a good characterization of their areal extent and an assessment of their drivers. The algorithm has been used to identify ozone episodes in Europe from April to September over the last twenty years (2003-2022) in the Copernicus Atmosphere Monitoring Service (CAMS) reanalysis. Episodes have also been detected in the historical simulation (1950-2014) and four shared socio-economic pathways (SSPs, spanning 2015-2100) of the United Kingdom Earth System Model (UKESM) for the purpose of providing future projections. While the total number of episodes has increased in recent years, the frequency of large episodes has decreased following European precursor emissions reductions. The analysis of the 100 largest episodes shows that they tend to occur in Northern Europe during spring and in the center and south of the continent from June onwards. Most of the top 10 episodes occurred in the first years of the century and were associated with anomalously high temperatures and anticyclonic conditions. Despite the decrease in large episodes in recent years, there is uncertainty regarding the fate of future European episodes. Episodes of reduced size are found for SSPs with weak

greenhouse forcing and low precursor emissions, whereas episode sizes increase in scenarios with high methane concentrations and enhanced radiative forcing, even exceeding the maximum historical size. This points to the need to implement effective climate and air quality policies to address the ozone air pollution problem in Europe in a warming climate.

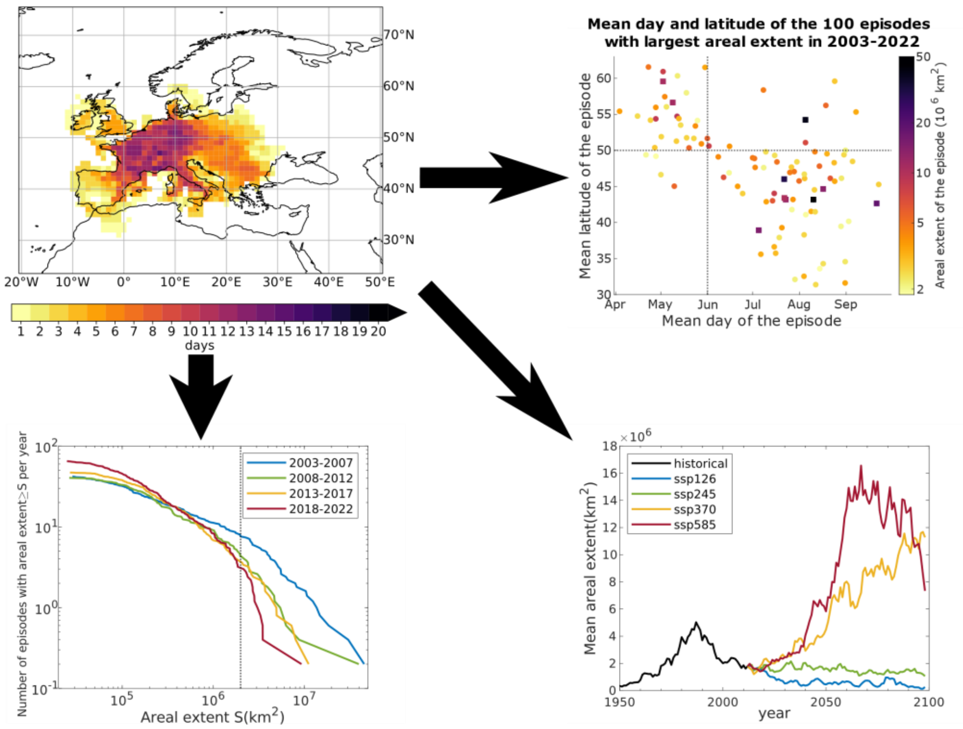

1. Introduction

Ozone (O_3) is produced in the troposphere by the photochemical oxidation of non-methane volatile organic compounds (NMVOCs), carbon monoxide (CO), and methane (CH_4) under the presence of nitrogen oxides (NO_x) and hydrogen oxide radicals (HO_X) (Sillman, 1999; Atkinson, 2000). Ozone remains from a few hours to days in the polluted boundary layer but has a longer lifetime of the order of weeks in the free troposphere, where it can be transported together with some of its precursors over intercontinental scales (Stevenson et al., 2006; Young et al., 2013; Monks et al., 2015), thereby contributing to baseline and near-surface ozone levels in distant regions (e.g., Lupaşcu and Butler, 2019; Derwent and Parrish, 2022).

Surface ozone concentrations are strongly dependent on meteorological conditions (Jacob and Winner, 2009; Fiore et al., 2012). Peak concentrations typically occur in the afternoon, often associated with high temperatures and clear-sky stagnant weather that favor photochemical production (e.g., Ordóñez et al., 2005; Leibensperger et al., 2008; Otero et al., 2016; Kerr et al., 2019; Porter and Heald, 2019). At high concentrations, ozone poses a serious threat to human health and the environment (Ashmore, 2005; Liu et al., 2018; GBD 2019 Risk Factors Collaborators, 2020), particularly when combined with other pollutants (Lian et al., 2022; Chen et al., 2024) or extreme heat (Willers et al., 2016; Otero et al., 2022). In 2015, exposure to ozone was estimated to cause 254,000 (95% uncertainty interval 97,000–422,000) deaths globally and 25,432 (7,356–53,160) premature deaths in Europe associated with respiratory diseases (Gu et al., 2023). Ozone is also considered the most detrimental air pollutant to vegetation and agricultural crops at the global scale (Tai et al., 2014; Tai and Val Martin, 2017; Feng et al., 2018).

Regional photochemical ozone production has declined over the last decades in Europe following precursor emission reductions (Monks et al., 2015; Karlsson et al., 2017). However, near-surface ozone concentrations have not decreased as the same rate as emissions (Karlsson et al., 2017; EEA, 2020), because of the non-linear nature of ozone chemistry (Kleinman et al., 2002; Sicard et al., 2020; Real et al., 2024) as well as the increasing influence of baseline concentrations in the free troposphere (Solberg et al., 2005; Monks et al., 2015; Derwent and Parrish, 2022). By contrast, European emission controls have reduced peak ozone concentrations and, therefore, the number of exceedances of air quality standards since the 1990s (EMEP/CCC, 2016; Colette et al., 2017; Derwent and Parrish, 2022; Real et al., 2024). Moreover, the slope of the ozone–temperature relationship during the warm season has decreased (Boleti et al., 2020; Otero, 2021). This has resulted in hot summers with lower ozone levels than expected, as found for instance in central Europe in 2018 (Zohdirad et al., 2022). Hence, all factors considered, regional precursor reductions appear to have been the primary cause of surface ozone changes in the last decades.

Nevertheless, obtaining a comprehensive picture of surface ozone changes over Europe is not straightforward, because most studies focus on a particular ozone metric, time period and region. For instance, different analyses have addressed baseline (Derwent et al., 2024), average (Boleti et al., 2018) or high percentile (Otero et al., 2022) ozone levels, which may have undergone opposite trends in recent years (Yan et al., 2018, 2019). The examination of different regions such as the Mediterranean (e.g., Sicard et al., 2013) or central Europe (e.g., Otero et al., 2021), or different local settings like rural and urban stations (Sicard et al., 2013; Yan et al., 2019), may also lead to contrasting conclusions. To overcome some of these limitations, recent studies have implemented different types of cluster analyses (Lyapina et al., 2016; Carro-Calvo et al., 2017; Boleti et al., 2020) that allow identifying regions or groups of stations where surface ozone follows coherent spatiotemporal patterns. This approach has proven useful in the evaluation and interpretation of model results (Lyapina et al., 2016), the assessment of long-term changes (Boleti et al., 2020) and the identification of meteorological drivers of ozone over different regions of the continent (Carro-Calvo et al., 2017). A limitation of these classifications is that they may be sensitive to changes in emissions and meteorological regimes.

Future ozone concentrations will also be determined by the combined effect of changes in precursor emissions and climate. As the effects of emission reductions may be locally variable depending on the chemical regime (Markakis et al., 2016; Liu et al., 2022b; Real et al., 2024), it is important to coordinate NO_x, NMVOC and methane controls to achieve lower ozone levels. On the other hand, it is expected that the increase in global mean temperatures will lead to higher ozone concentrations during the peak season in polluted regions, potentially eroding the benefits of emission controls. This effect has been termed the ozone climate penalty (Bloomer et al., 2009; Rasmussen et al., 2013). Different mechanisms triggered by climate change can impact the climate penalty (Colette et al., 2015; Fu and Tian, 2019), thus altering the response of ozone to projected warmer temperatures (Kerr et al., 2019; Porter and Heald, 2019; Archibald et al., 2020b; Otero et al., 2021). Overall, climate change is expected to increase ozone levels over regions close to pollution sources and decrease them in regions remote from pollution sources (Zanis et al., 2022), but there is considerable variation depending on the scenario.

Some studies (e.g., Colette et al., 2015; Orru et al., 2019) have projected a larger effect of regional precursor emission reductions compared to that of the climate penalty during the 21st century over Europe. Others (e.g., Fortems-Cheiney et al., 2017) have concluded that the benefits of those reductions could be annihilated by high background ozone concentrations caused by increases in global methane amounts. Analyses of CMIP6 (Coupled Model Intercomparison Project Phase 6) projections under different Shared Socioeconomic Pathways (SSPs) show that future near-surface ozone changes over different regions of the globe strongly depend on the scenario, and that strict air quality policies may be needed to keep ozone below current levels under high greenhouse forcing (Turnock et al., 2020, 2022).

While some global modelling studies have projected future changes in the monthly, seasonal, or annual means of ozone (Turnock et al., 2020, 2022; Liu et al., 2022a; Zanis et al., 2022), others have also addressed changes in the afternoon ozone mixing ratios (Karlsson et al., 2017; Liu et al., 2022b). Their results are not directly comparable, because the shape of the diurnal ozone cycle often depends on the meteorological conditions (Garrido-Perez et al., 2019). On the other hand, addressing past and future changes in ozone extremes is needed for improved assessments of air quality policies and ozone-related health impacts. These extremes occur predominantly as organized, multiday episodes with coherent spatiotemporal patterns and spatial extents of more than 1000 km (Schnell et al., 2014, 2015), reflecting that the build-up of ozone typically takes place within large, slow-moving, stagnant, high-pressure systems over several days. Identifying such spatiotemporal structures goes beyond site-type or regional classifications (Lyapina et al., 2016; Carro-Calvo et al., 2017; Boleti et al., 2020), which may not be stable over long time horizons.

In this work we present a new semi-Lagrangian algorithm that enables the identification of large-scale ozone episodes and the characterization of their spatiotemporal patterns, with the aim of assessing past and future changes in afternoon ozone episodes over Europe during the warm season. For this purpose, we have used a recent 20-year period of the Copernicus Atmosphere Monitoring Service (CAMS) reanalysis and future projections of the United Kingdom Earth System Model (UKESM). The paper is structured as follows: Section 2 is dedicated to the description of the datasets and the algorithm; Section 3 presents a catalogue of European ozone episodes in CAMS and discusses the observed changes, with a focus on the largest ozone episodes, and Section 4 assesses future changes in large ozone episodes in UKESM under different CMIP6 scenarios. Finally, Section 5 concludes with a summary of the main findings.

2. Data and methods

2.1 Data

For the identification of extreme ozone episodes over the last years, we have used 20 years (2003-2022) of 3-hourly ozone mixing ratios from the CAMS reanalysis (Inness et al., 2019) over a domain covering Europe [20° W–50° E; 25°–75° N] at 1° x 1° horizontal resolution (Figure 1a). Maximum daily 8-hour average (MDA8) is the primary ozone standard in the European Union (European Commission, 2008), and is commonly used in many studies concerning ozone air pollution (e.g., Travis and Jacob, 2019, and references therein). Nonetheless, as the MDA8 metric cannot be computed from 3-hourly data, we have extracted the daily maximum concentrations over each grid cell from CAMS.

For some of the analyses, we have used a 1°x1° hourly gridded ozone dataset over a limited European domain [13° W–34° E; 36–70° N], covering the period from 2003 to 2015 (Schnell et al., 2014, 2015). This dataset was created by interpolating and merging observations from the European Environment Agency's air quality database (AirBase) and the European Monitoring and Evaluation Programme (EMEP) with the objective mapping algorithm presented by Schnell et al. (2014). Overall, the daily ozone maxima provided by CAMS exhibit little discrepancy with the values from observations in the overlapping area of both datasets, accurately reproducing the amount of surface ozone (see Supplement S1).

We have also assessed the evolution of O_3 episodes in the historical simulation (1950-2014) and future projections under four Shared Socioeconomic Pathways (ssp126, ssp245, ssp370 and ssp585, 2015-2100) from UKESM version 1 (UKESM1-0-LL, referred to as UKESM1 hereafter; Sellar et al., 2019; Archibald et al., 2020). Daily O_3 maxima from these simulations (variant r1i1p1f2), conducted as part of CMIP6, have been downloaded from the Earth System Grid Federation (ESGF) database. The data, available with a horizontal resolution of 1.875° latitude x 1.25° longitude, have been interpolated to 1° x 1° over the same European domain used for the CAMS reanalysis. We have restricted our analyses (for the CAMS reanalysis, the gridded observational dataset and UKESM1) to the daily O_3 maxima from the months of April through September, which coincide with the period when ozone concentrations are typically highest on the continent (Scheel et al., 1997; Monks, 2000; Aggelis et al., 2013; supplementary of Ordóñez et al., 2020).

To understand the evolution of O_3 episodes in time scales of years, we have used monthly anthropogenic emissions of some ozone precursors (CO, NO_x, and NMVOCs) from the CAMS reanalysis. We have also examined the concentrations of CH_4 at the lowest model level, which are prescribed as boundary conditions in the CAMS reanalysis (Flemming et al., 2015; Huijnen et al., 2022). Monthly data of emissions of these precursors, in addition to atmospheric concentrations of CH_4 and daily maximum temperatures at the lowest model level, have also been extracted for the historical simulations and future scenarios of UKESM1.

Finally, to study the relationship between the largest ozone episodes in the CAMS reanalysis and synoptic conditions, we have extracted daily maximum temperatures and geopotential height at 500 hPa (Z500) from the ERA5 reanalysis (Hersbach et al., 2020) at 0.75° x 0.75° horizontal resolution.

2.2. Local ozone extremes

Before detecting large-scale ozone episodes (i.e., periods of anomalously high atmospheric mixing ratios of near-surface ozone extended in space and time, typically spanning thousands of square kilometers over several days), we identified local extreme ozone events (local O_3 events hereafter). For each grid cell, a local O_3 event is found if the daily maximum ozone exceeds a certain threshold. The first practical question that arises is whether to use relative (exceedances of a value determined by a percentile in each cell) or absolute thresholds (exceedances of a fixed value). Relative thresholds may be preferred over absolute ones because they enable a better exploration of the relationship between ozone episodes and the associated synoptic conditions (Schnell et al., 2014). This happens because exceedances of absolute thresholds are often found in regions with high baseline ozone concentrations regardless of the synoptic conditions. Moreover, relative thresholds may be appropriate to minimize the effect of model biases in reproducing the observed O_3 concentrations. However, relative thresholds are not as good a measure of health risk as for other variables like temperature (Curriero et al., 2002; McMichael et al., 2006; Kovats and Hajat, 2008; Lass et al., 2011), because organisms do not adapt to ozone. Indeed, as the effects of ozone exposure on mortality and morbidity begin to appear at certain concentrations (e.g., Horstman et al., 1989), most impact health assessments for this pollutant rely on absolute thresholds (e.g., Orru et al., 2013; Archibald et al., 2018; Fenech et al., 2018).

According to the EU air quality directive (2008/EC/50), the target value for ozone for the protection of human health is based on MDA8 concentrations, which should not exceed 120 μg/m^3 (~60 ppb) on more than 25 days per calendar year averaged over three years (European Commission, 2008). From the analysis of the observational gridded ozone dataset, we found that this absolute threshold corresponds to daily O_3 maxima ranging from 61 to 67 ppb, depending on the latitude, during April-September. This range is reduced to around 61-64 ppb daily O_3 maxima corresponding to 60 ppb MDA8 O_3, following a polynomial fitting that minimizes the effect of poor observational coverage over some regions (see Supplement S2).

Some grid cells in the southern part of the domain in CAMS often exhibit daily maximum ozone mixing ratios well above the considered absolute threshold for that latitude (~61–64 ppb). For example, the 95th local percentiles exceed 80 ppb over the Po Valley and some parts of the Mediterranean (Figure 1a). Consequently, prolonged ozone episodes exceeding the absolute threshold could often be found over those regions. On the other hand, the 95th percentiles of daily O_3 maxima are close to (and even exceed) the absolute threshold over most of continental Europe south of 50° N and start to decrease rapidly to the north. Given such geographical disparities, we have chosen to use relative thresholds to select local ozone extremes, in particular the local 95th percentiles of daily ozone maxima in April-September 2003-2022 (i.e., ~9 days per ozone “season”, ~91 days per decade). This has the advantage of providing ozone extremes that can be related to the synoptic conditions and, at the same time, correspond to hazardous ozone concentrations in a broad region of Europe, allowing for the assessment of the impacts. This choice also aligns with criteria applied in prior studies (Otero et al., 2016, 2022; Carro-Calvo et al., 2017). Finally, we have applied a land-sea mask to disregard the local O_3 events that appear over grid cells entirely located in the ocean, as they do not pose a risk to the population. This does not affect the identification of ozone episodes (Sect. 2.3) that cover nearby regions separated by the sea, such as the British Isles and France, because of the 1°×1° grid size used in this work. CAMS shows good skill in identifying local O_3 events, especially in regions with high density of monitoring sites (see Figure S2).

Similarly, we have identified local ozone events over land areas of the same domain in UKESM1 as exceedances of the local 95th percentiles in April-September of the last twenty years of the historical simulation (1995-2014, see Figure 1b). This period is used as a reference to compare the evolution of O_3 extremes both in the historical simulation and in future scenarios. Due to the known overestimation of summer surface ozone in models (Turnock et al., 2020), the 95th percentiles obtained for the last twenty years of the historical simulation correspond to considerably higher ozone mixing ratios than in CAMS for most of Europe. These large differences between CAMS and UKESM1 remain if both datasets are evaluated for a common period (Figure S6), strongly supporting the choice of a relative threshold as discussed above. Despite these differences, the ozone mixing ratios corresponding to the 95th percentiles in northern Europe are much lower than in the rest of the continent for both datasets, never exceeding 60 ppb north of 60° N. Indeed, this would prevent the identification of extremes if they were defined based on an absolute threshold (i.e., 60 ppb MDA8).

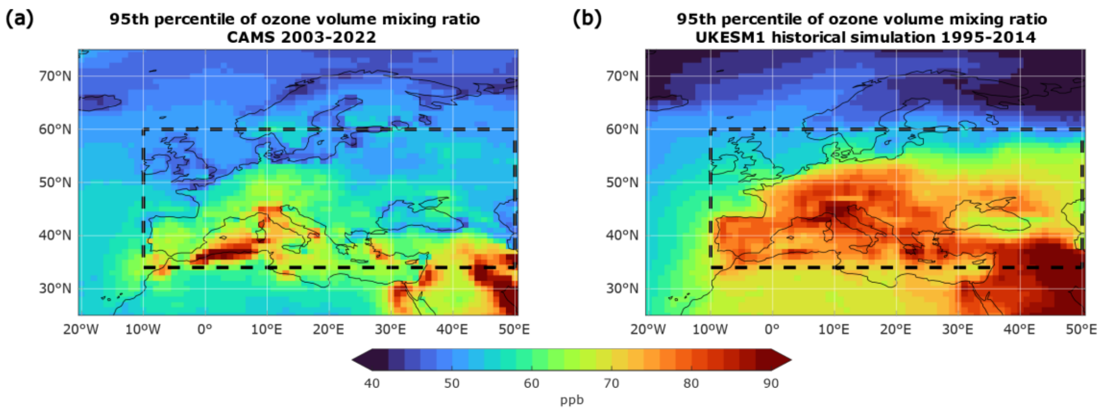

Figure 1: *95th percentiles of the daily maximum ozone volume mixing ratios in Europe obtained from (a) the CAMS reanalysis during April-September from 2003 to 2022 and*

from (b) UKESM1 historical simulation during April-September from 1995 to 2014. The black dashed box covers the reduced domain [10° W–50° E; 34–60° N] where the characteristics of ozone episodes are assessed.

Concluding, local O_3 events have been detected in CAMS and UKESM1 as exceedances of local 95th percentiles over each land grid cell of the domain shown in Figure 1, i.e. [20° W–50° E; 25°–75° N], referred to hereafter as the extended domain. As these percentiles correspond to low mixing rations in northern Europe, we will limit some of the subsequent analyses to a reduced domain ([10° W–50° E; 34–60° N], see black dashed box in the figure). This encompasses the most populated regions of Europe and the land areas where ozone may pose a risk to human health.

2.3. Pseudo-Lagrangian algorithm to track and characterize ozone episodes

Starting from the local O_3 events obtained in Sect. 2.2, we have developed an algorithm that builds on others previously used for the detection of organized, large-scale, multiday ozone episodes (Schnell et al., 2014) and heatwaves (Sánchez-Benítez et al., 2020). In that spirit, the algorithm presented in this section groups the local ozone extremes in aggregations of adjacent events called clusters, in such a way that all the events forming the same cluster are connected in space and time. For each day, we define daily patterns as sets of all local events in the same cluster occurring on that specific day. Finally, we obtain a set of separate ozone episodes (over the extended domain of Figure 1), each of them defined as a cluster which has been fully processed by the algorithm as follows (see also the schematic flowchart in Figure 2, and an example of the algorithm output in Figure S7):

- The algorithm groups the local O_3 events in clusters. An O_3 event is included in a cluster if the maximum coordinate distance to the nearest event in that cluster is equal to or less than one degree in longitude and latitude, and equal to or less than one day in time. Thus, this first step yields numerous clusters that can last several days. Each one encompasses a sequence of consecutive daily patterns that include all local events within that cluster on a given day.

- Grouping O_3 events by a maximum cut-off coordinate distance has some limitations. The procedure considers time as another dimension in addition to latitude and longitude, such that the distance of 1° is equivalent to that of 1 day. On certain days, this may result in the appearance of spatially disconnected aggregations of events, sometimes yielding incoherent daily patterns. To address this problem, the second step of the algorithm selects the main body of each daily pattern, i.e., the largest aggregation of connected events considering only those in the reduced domain of Figure 1. Then, it removes all structures that are disconnected from the resulting pattern. Consequently, the number of clusters remains unchanged but now with coherent daily patterns.

- Some of the resulting clusters may consist of successive slightly overlapping daily patterns. To prevent their categorization as a single episode, the algorithm includes a third step which splits a cluster into two distinct episodes on a given day if the shared area with the daily pattern of the previous day is less than 50%. We should note that advection of polluted air masses has been associated with summer ozone pollution over some parts of Europe (e.g., Carro-Calvo et al., 2017), which might cause abrupt changes in the spatial patterns between two consecutive days. Because of that, we have adopted an additional condition that relaxes the required 50% minimum overlap to only 20% if the distance between the centers of two daily patterns is less than 500 km, similarly as done by Sánchez-Benítez et al. (2020) for the detection of heat waves.

- The cluster is also truncated on a given day if the total area of the corresponding daily pattern is less than 250,000 km^2, unless that day falls among the two earliest or two latest days of the episode. This way, the algorithm identifies large-scale episodes while providing flexibility for episode formation and dissipation in a similar way as done by Schnell et al. (2014).

- Finally, we retain only the clusters that affect the reduced domain for at least three days.

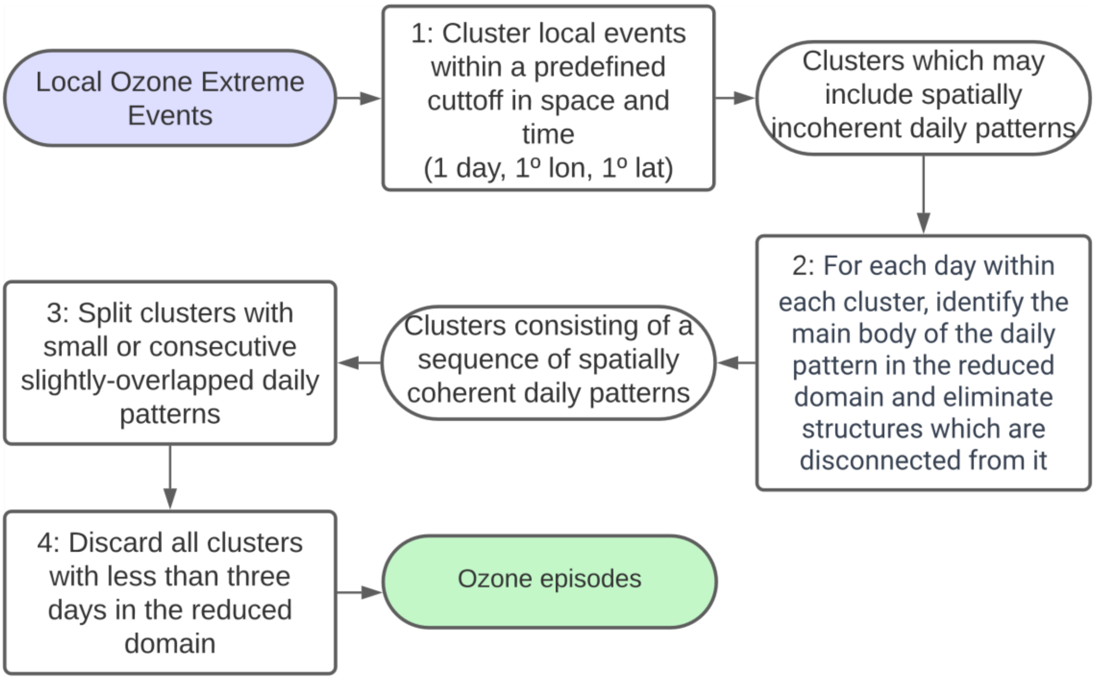

Figure 2: *Flowchart of the ozone episode detection algorithm.*

It should be noted that, while the focus of this study is on ozone episodes over the reduced domain [10° W-50° E; 34-60° N], where the highest concentrations are typically found, the algorithm identifies and groups events over the extended domain [20° W-50° E; 25°-75° N]. This way we avoid truncating episodes that may be partially over the main area of interest. Then we have used the total accumulated areal extent (areal extent hereafter) as the main metric to characterize ozone episodes over the reduced domain. This is computed as the aggregate of the areas of the daily patterns (considering only cells in the reduced domain) throughout the length of an episode, i.e.,

$$area = \sum_{d} \sum_{i,j} area_{i,j,d} \quad (1)$$

with $area_{i,j,d}$ being the area of the cell (i,j) where a local O_3 event was found on day d.

Additionally, a metric based on the ozone enhancement over a specific threshold was considered to quantify the magnitude of the episodes but finally was discarded for two reasons. First, it added little information to that obtained from the areal extent, as both metrics were highly correlated (they scaled in a similar way with the number of local events included in the episode). Second, the CAMS reanalysis was found to heavily overestimate ozone mixing ratios in specific circumstances, such as wildfires (Figure S3), thus causing this metric to overestimate the magnitude of some episodes.

3.Catalogue of European ozone episodes in 2003-2022

We found a total of 974 episodes in the CAMS reanalysis during April-September 2003-2022, ranging from 3 to 30 days of duration, and with areal extents from $2.5\cdot10^4$ to $4.6\cdot10^7$ km^2 over the reduced domain. The number of ozone episodes has increased towards the end of the period (blue line in Figure 3a). For example, they ranged from 32–51 episodes/year in the first five years to 52–80 episodes/year in the last five years of the reanalysis. The year with the highest number of episodes was 2018, which has already been reported to have several ozone episodes associated with an intense heat wave (Pope et al., 2023), although ozone levels were not as high as expected for such a warm summer due to European reductions in precursor emissions (Zohdirad et al., 2022). This is also the April-September period with the highest daily maximum temperatures averaged over the reduced domain (Figure S10).

The rise in the number of episodes might be due to increasing large-scale, high-impact episodes, to an incremented occurrence of small episodes, or to both. To understand this in detail, we examined the number of episodes exceeding different areal extents in each 5-year subperiod (i.e., 2003-2007, 2008-2012, 2013-2017, and 2018-2022). The analysis reveals that the number of large episodes per year has decreased, as shown in Figure 3b. For instance, during 2003-2007 (blue line in that panel), there were approximately 8 episodes per year (on average) with a minimum size of $2 \cdot 10^6$ km^2 (vertical dotted line). This corresponds to the areal extent of the 92nd largest episode in the whole 20-year period. The frequency of episodes of that size has more than halved in later subperiods. They decreased to approximately 4 per year in 2008-2012 (green line) and about 3.5 and 3 per year in the two most recent subperiods (yellow and red lines). The results are significantly impacted by the summer of 2003, when several extreme episodes (among the top 10) occurred, as will be shown in Section 3.2. Conversely, the number of small episodes has increased in recent subperiods, outweighing the decrease in larger ones. As a result, there is a net increase in the total number of episodes (blue line in Figure 3a).

Furthermore, Fig. 3c depicts the complementary cumulative distribution functions of the areal extent (i.e., the percentage of the total areal extent found in episodes greater than or equal to a certain areal extent) for each 5-year subperiod. It becomes evident that the relative weight of large episodes with respect to the total episode area has decreased gradually since 2003. From 2003 to 2007, more than 80% of the total area of all ozone events was found in episodes larger than $2 \cdot 10^6$ km^2 (vertical dotted line). For later years, that percentage was reduced to approximately 60%, 50% and 35% in the 2008-2012, 2013-2017 and 2018-2022 subperiods, respectively.

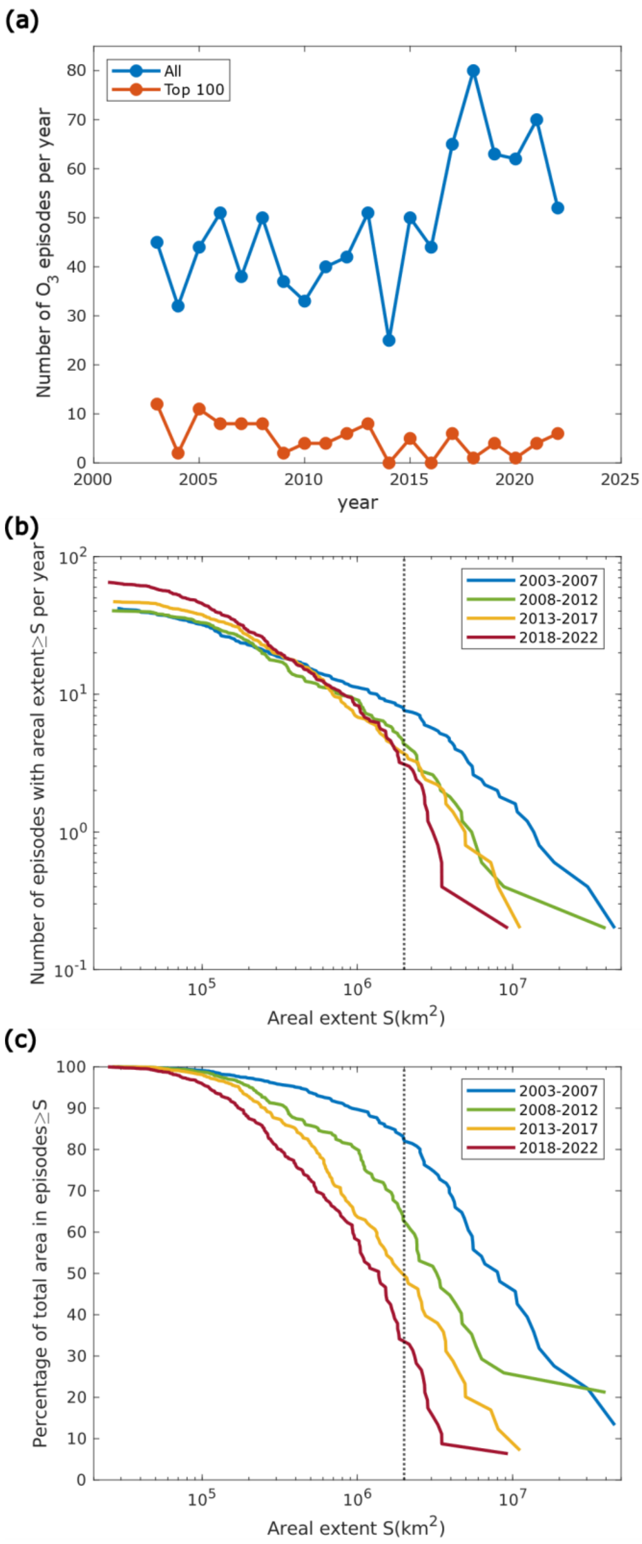

Figure 3: *(a) Total number of ozone episodes (blue line) and number of ozone episodes among the top 100 (orange line) found for the CAMS reanalysis in each April-September period of 2003-2022. (b) Number of episodes per year (y axis) exceeding a given areal*

extent (x axis) for each five-year subperiod. (c) Percentage of the total areal extent (y axis) found in episodes greater than a given size (x axis) for the same subperiods.

Based on these analyses, it can be concluded that large-scale ozone episodes are becoming less frequent in Europe. This could be expected from the strong decline in regional anthropogenic precursor emissions in the last twenty years over Europe, which has not been compensated for by the rising temperatures and the moderate increases observed in methane concentrations (Figures S10 and S11). The reduction in precursor levels has resulted in a decreasing number of local ozone events, which becomes more apparent when considering only those grouped in ozone episodes (Figure S12). It appears that towards the end of 2003–2022 local events have more difficulties to merge into organized episodes than at the beginning of that period, resulting in the emergence of smaller, scattered episodes. This could explain the apparent contradiction between the rise in the total number of episodes and the decline in the larger ones (Figure 3a). These results are consistent with those from previous studies (Sicard et al., 2013; Paoletti et al., 2014; Boleti et al., 2020; Otero et al., 2021; Zohdirad et al., 2022; Real et al., 2024), which support the effectiveness of emission reduction policies in tackling peak ozone concentrations in Europe and highlight the need to maintain these actions in the future.

In the remainder of the section, we will examine the temporal evolution and latitudinal distribution of the top 100 episodes as well as the main features of the top 10 episodes in 2003-2022.

3.1. Top 100 episodes in 2003-2022

The number of episodes among the top 100 (orange line in Figure 3a) have decreased at a rate of -3.0 ± 2.5 episodes/decade (linear trend with 95% confidence interval, p-value = 0.022). In each of the first five years – excluding 2004, for which significant biases were reported in CAMS by Inness et al. (2019) – 8 to 12 episodes were identified among the top 100, while only 1 to 6 episodes were found in each of the last five years. This result is in line with the decrease in large episodes reported above.

Furthermore, we have investigated the typical timing and location of these episodes. For this purpose, Figure 4 shows the average calendar day and mean latitude for the 100 largest episodes. This analysis is motivated by previous reports on the occurrence of episodes in the north of Europe during spring (Monks, 2000; Monks et al., 2015; and references therein), which could extend to lower latitudes. Keeping such episodes in mind, not considering cells north of 60° N may result in a bias in the temporal-latitudinal dependence. Because of that, we have also included cells outside the reduced domain [10° W–50° E; 34–60° N] to calculate the mean latitude and day of each episode.

We have found that 60 of the top 100 episodes occurred south of 50° N between June and September, 31 episodes during April and May (27 of them north of 50° N and only 4 to the south), and the remaining 9 north of 50° N between June and September. Therefore, there is a clear prevalence of large summer episodes over most of the continent, but with spring episodes happening mostly in the North. Around two thirds of these episodes are found in the first 10 years of the CAMS reanalysis (2003–2012) and the remaining third in 2013–2022 (Figure S3). Compared to the whole 20-year period, the last decade shows an even stronger preference for spring episodes in the north and summer episodes south of 50° N, but with a notable decline in the latter while the number of spring episodes remains barely unchanged.

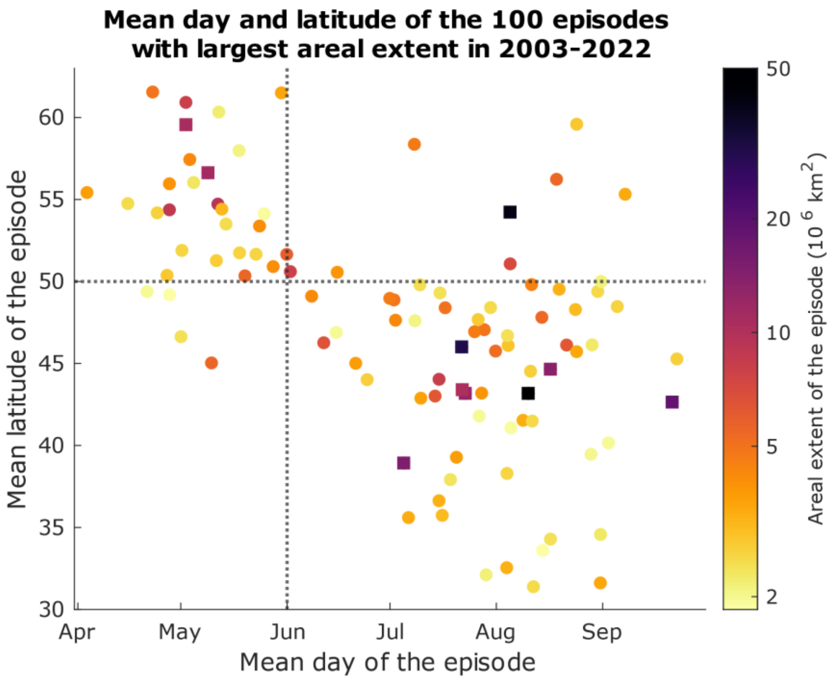

Figure 4: *Mean day and mean latitude for each of the 100 largest European ozone episodes in the CAMS reanalysis (2003– 2022). The colors of the markers show the area of the episode. The 10 episodes with greatest area (see Section 3.2) are represented with square markers. The dotted horizontal line marks 50° N, separating the north and center-south of Europe, whereas the dotted vertical line is placed at the beginning of June, separating the first two months in the extended summer (April-September) from the rest.*

The distribution of the largest episodes in latitude and calendar day over the whole period of analysis is coherent with the occurrence of conditions that favor ozone production during summer, such as stagnation, elevated temperatures, and high solar radiation (Jacob and Winner, 2009; Otero et al., 2016; Carro-Calvo et al., 2017), which are more severe in the center and south of the continent than in the north. On the other hand, the reasons behind the high occurrence of ozone episodes in northern Europe during spring remain unclear despite some efforts to understand this behavior. Several phenomena have been proposed as possible candidates, including dynamical processes such as stratosphere-to-troposphere transport, and enhanced photochemistry, the latter consuming precursors accumulated during winter (Oltmans, 1981; Penkett and Brice, 1986; Monks, 2000; Monks et al., 2015; Sarwar et al., 2024). To date, there has been no clear attribution to any of these processes. Further studies in that direction could explain the apparent lack of reduction in spring northern episodes as compared to summer episodes in central and southern Europe in later years (Figure S13). Nonetheless, the most extreme episodes were co-occurrent with anticyclonic and temperature anomalies even in the north of Europe, as will be shown in the next subsection.

3.2. Top 10 ozone episodes in 2003-2022

The ten largest European ozone episodes since 2003, ranked by their areal extent over the reduced domain in CAMS, are presented in both Figure 5 and Table S1. Most of them correspond to well-documented heatwave conditions in the literature. These episodes were associated with concurrent positive anomalies of both Z500 (i.e., anticyclonic conditions) and daily maximum temperature (See Figures S8 and S9), which favor the photochemical production of ozone.

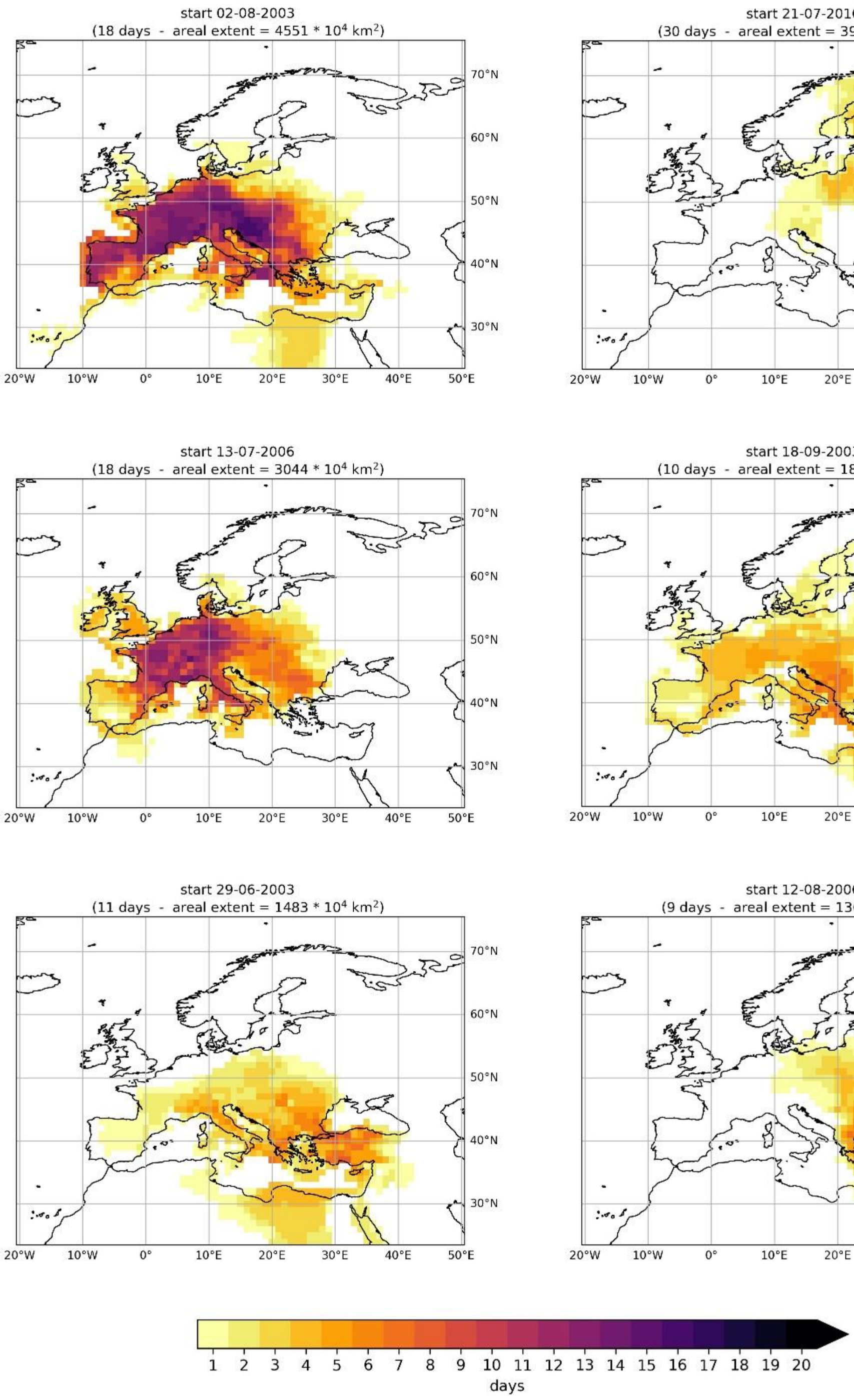

Figure 5: *Local frequencies (number of days over each CAMS grid cell) of the top 10 European ozone episodes according to their areal extent over [10° W-50° E; 34°-60° N] in April-September 2003-2022. The start date, duration, and areal extent of each episode are indicated on the top of the respective panel.*

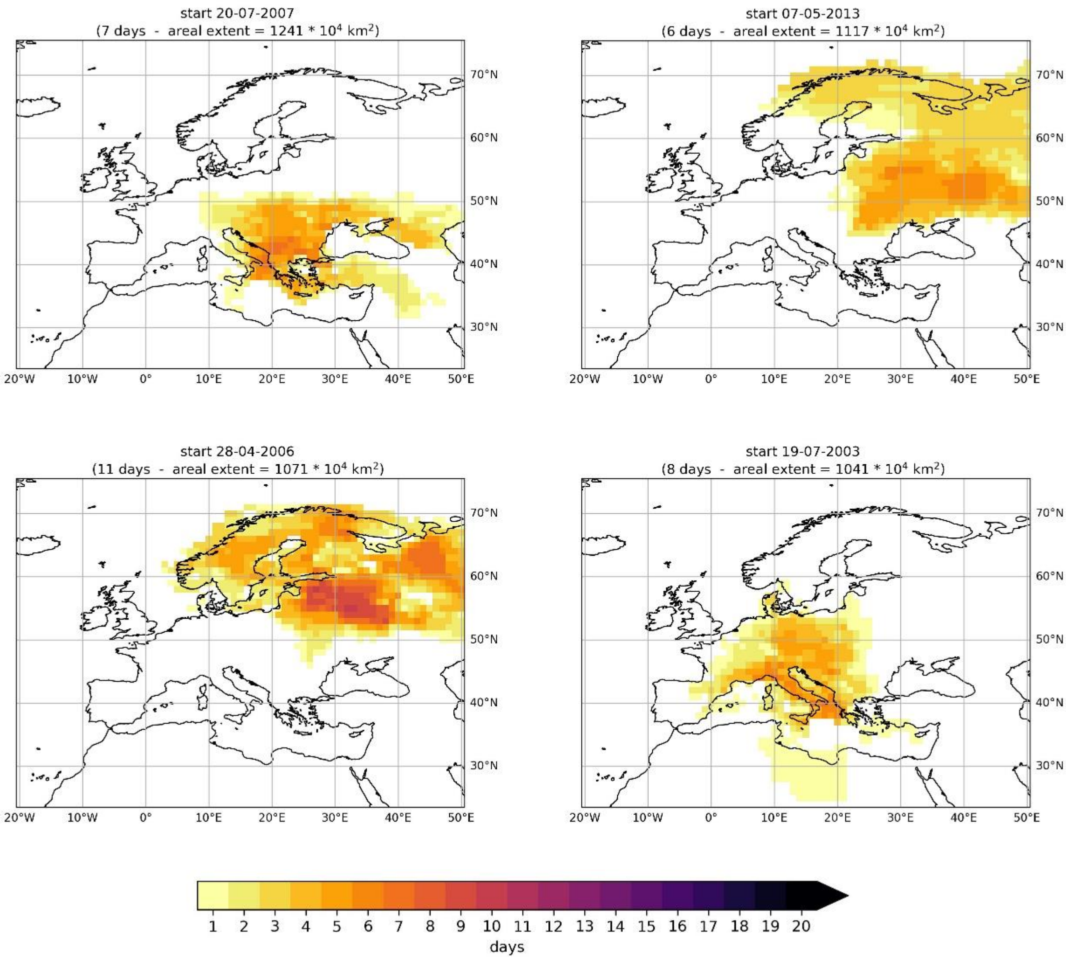

Figure 5: *Continued.*

Summer 2003, unprecedented in Europe at that time (Garcia-Herrera et al., 2010), had four episodes among the top ten. The episode in the first half of August stands out as the largest one in the CAMS reanalysis period. It coincides with the mega-heatwave that affected western Europe in August 2003, which featured strong meteorological anomalies, caused thousands of heat-related deaths and led to poor air quality (e.g., Trigo et al., 2005; Vautard et al., 2005; Solberg et al., 2008; Ordóñez et al., 2010; Russo et al., 2015). The other three episodes found in 2003 (June-July, July, and September) were also related to positive Z500 and temperature anomalies, although they were weaker than those during the great episode of August (Figure S9).

The second largest episode occurred in western Russia during summer 2010. This is also the longest one by far, spanning 30 days. It affected regions outside the reduced domain (north of 60° N) which are not accounted for in the calculation of the areal extent. Otherwise, it would have been ranked as the largest episode, surpassing that of August 2003. This episode coincided with a well-known mega-heatwave that broke 500-year temperature records, an event considered unprecedented even in comparison to the 2003 heat wave (Barriopedro et al., 2011; Russo et al., 2015). The extreme temperatures and wildfires during that heatwave resulted in extremely severe air pollution in several Russian regions (Konovalov et al., 2011).

The third-largest episode happened in 2006 (see its evolution in Figure S7). It was associated with the central-western European heatwave of July 2006, caused by an omega blocking pattern in the region (Rebetez et al., 2009; Russo et al., 2015). This year has previously been identified as one of the years with the highest number of ozone extremes (Schnell et al., 2014; Carro-Calvo et al., 2017). Another episode of summer 2006 found among the top 10 (top 6) affected the Balkans and eastern Europe during August. It was related to a heatwave that ended at the same time as devastating wildfires began in Greece (Vlachou et al., 2010; Climate Action Network Europe, 2013). Additionally, a smaller episode among the top 10 (ranked 9^{th}) took place in northern Europe in the spring of the same year. It was associated with atmospheric blocking, abnormally warm temperatures for that time of the year, and smoke from biomass burning transported northward from Eastern Europe, breaking air pollution records in Scandinavia (Stohl et al., 2007; Hall and Loboda, 2018).

The two remaining episodes also correspond to periods when synoptic conditions favored the occurrence of well-documented heatwaves. These include the heatwave in the Balkans during July 2007 (Founda and Giannakopoulos, 2009; Russo et al., 2015), which resulted in high ozone concentrations in the region (Carro-Calvo et al., 2017), and the second warmest May on record in Russia in 2013 (The Moscow Times, 2013; NOAA, 2013).

In line with the previous results, the most extreme ozone episodes are also becoming less frequent in the most recent years. Eight of the top 10 happened during the first five years of the period of study (2003-2007). Only one (though massive) episode was found in the second 5-year subperiod and the last one happened in 2013, despite several record-breaking summers and severe heatwaves affecting Europe in the last decade (Barriopedro et al., 2020, 2023; Sousa et al., 2020; Zohdirad et al., 2022). These include the summer of 2022, which was the hottest on record in Europe (Copernicus, 2022; Ballester et al., 2023), and the summer of 2018, one of the warmest on record (Copernicus, 2018; Rousi et al., 2023). Note also that 2018 was the year with highest average daily maximum temperatures over the extended summer in the continent (Figure S10).

It can be concluded that the ten largest ozone episodes in Europe were associated with heat waves, as could be expected because both are driven by similar synoptic conditions. On the other hand, recent episodes, although more frequent (Figure 3a), are becoming smaller following the decline in organized local extremes over the last years (Figure S12). Therefore, the overall reduction in European precursors (Figure S11) has had a greater impact on ozone extremes than the warming climate (Figure S10), resulting in an overall decrease in the frequency and extent of large-scale ozone episodes.

4. Projections of future European ozone episodes

The results obtained for the CAMS reanalysis show a reduction in large episodes over the period 2003–2022. However, it is unclear whether this reduction will continue in the future, because the emissions of ozone precursors and the level of climate forcing vary considerably among the different CMIP6 scenarios. Hence, we have applied the algorithm to identify O_3 episodes in the historical simulation and four future scenarios (ssp126, ssp245, ssp370 and ssp585) simulated by UKESM1.

As indicated above (Sect. 2.2), local O_3 extremes are identified as exceedances of the grid cell 95th percentiles in April-September over the last 20 years of the historical simulation (1995–2014). Then ozone episodes are tracked from 1950 to 2100. We examine the evolution of both the mean area of all episodes and the mean area of large episodes, namely those with areas above the 90th percentile, in 5-year moving windows (Figure 6). The choice of the 90th percentile as a threshold for large episodes aligns with the analysis of the top 100 episodes presented in the previous section, which roughly correspond to that percentile (100 out of a total of 974 episodes found for CAMS). Note that the historical simulation finishes in 2014 and the four SSPs start in 2015. Because of this, the mean areas of the historical simulation shown in Figure 6 are calculated for windows until 2010-2014, while windows from 2011-2015 through 2014-2018 incorporate data from both the historical simulation and their respective SSP, and windows from 2015-2019 onwards only include data from the SSPs.

The areal extent of both average and large episodes increased until the 1980s and decreased from the 1990s onwards in the historical simulation. This decline is in accord with the decrease in large episodes observed for the CAMS reanalysis. However, the projections of these episodes diverge considerably across the different SSPs. Episodes decrease in size during the first years in the scenario with weakest greenhouse forcing (ssp126) and show a very slight decrease during the second half of the century for ssp245. On the other hand, there is a clear increase in projected sizes for the two scenarios with the strongest greenhouse gas forcing (i.e., ssp370 and ssp585), breaking the historical records consistently after 2050. The worst-case scenario (ssp585) exhibits large interannual variability after 2060 though.

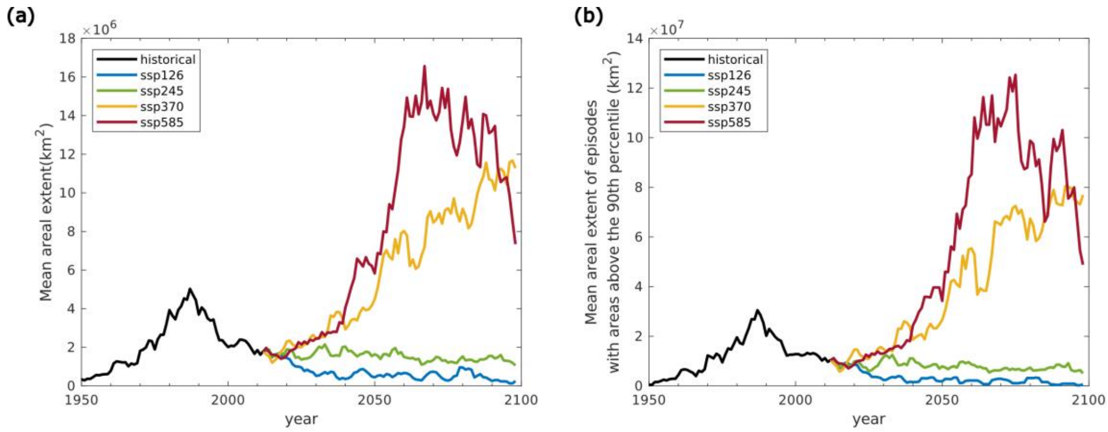

Figure 6: *Evolution of the mean areal extent of (a) all episodes and (b) those with areas above the 90th percentile in 5-year rolling windows centered on each year over [10° W-50° E; 34°-60° N] for the historical simulation (1950-2014) and four CMIP6 scenarios (2015-2100) of UKESM1.*

To understand the long-term variations in ozone episodes for the different scenarios, we have examined changes in daily maximum temperature (Figure 7) and the main O_3 precursors (Figure 8). European temperatures start rising steadily since around 1980 in the historical simulation and continue this trend (although at different rates depending on the scenario) during the 21st century, stabilizing after 2050 only in ssp126. This is consistent with large episodes becoming more prominent in ssp370 and ssp585, but not with the declines observed in the historical simulation and in the other two scenarios. Methane concentrations increased slightly during the last two decades of the historical simulation. A similar increase can be observed in total VOC emissions, which include biogenic emissions of isoprene and terpenes (calculated interactively by the model), despite reductions in the relatively minor anthropogenic component. Therefore, the reduction in the size of ozone episodes since the early 1990s must be attributed to the strong declines in NO_x and CO emissions.

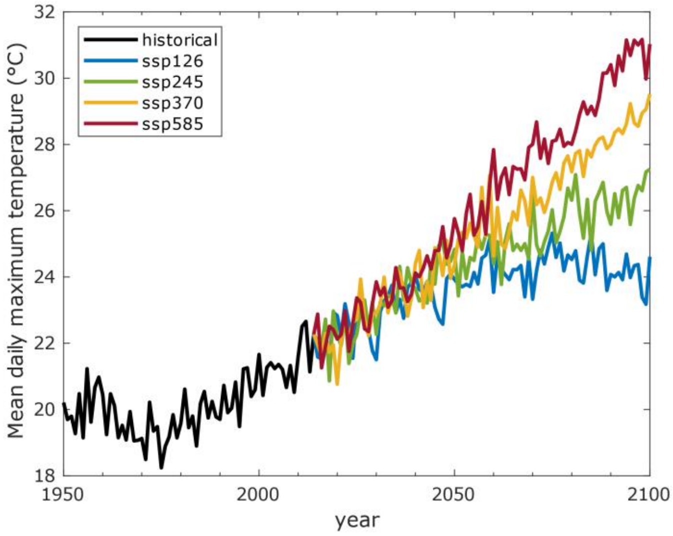

Figure 7: *Daily maximum temperatures at the lowest model level averaged over the domain [10° W–50° E; 34–60° N] during April-September for each year of the historical simulation (1950-2014) and four scenarios (2015-2100) of UKESM1.*

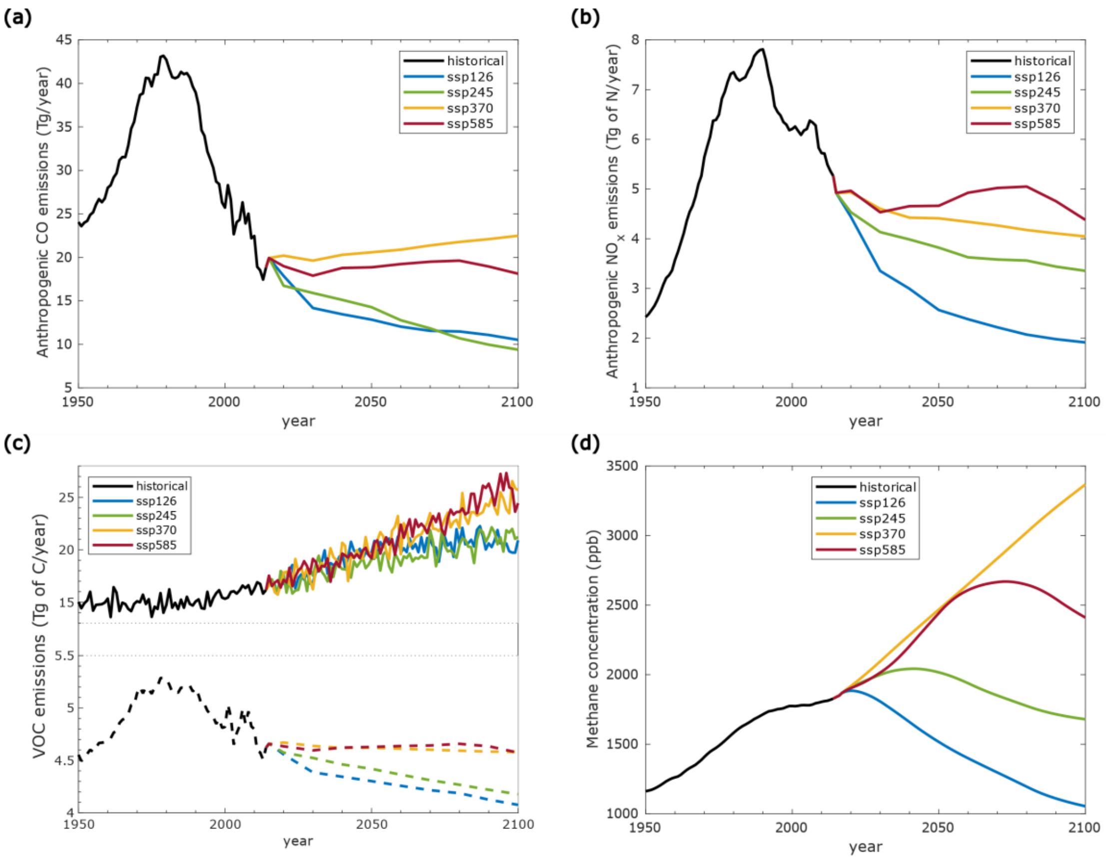

Figure 8: *Evolution of April-September anthropogenic emissions of (a) CO and (b) NO_x as well as (c) anthropogenic (dashed line) and total (solid line, biogenic plus anthropogenic) NMVOC emissions over the domain [10° W–50° E; 34–60° N] for each year of the historical simulation (1950-2014) and four CMIP6 scenarios (2015-2100) of UKESM1. (d) As the other panels, but for CH_4 concentrations at the lowest model level.*

Future VOC emissions rise in all future scenarios, particularly in those with higher climate forcing. This is due to the overall positive responses of biogenic emissions to high temperatures, as anthropogenic VOC emissions decrease (for ssp126 and ssp245) or remain almost unchanged (in the high forcing scenarios). Nevertheless, there are clear differences for the other precursors. The strong decline in NO_x, CH_4 and, to a lesser extent, CO from the first years of the ssp126 scenario outweighs the impact of a warming climate, causing a decrease in the size of ozone episodes. Compared to ssp126, NO_x and CH_4 decreases are much less pronounced and tend to be delayed into the 21st century, and temperature increases are sustained until the end of the century in ssp245.

Despite the moderate but steady decline in NO_x and CO emissions in this scenario, methane concentrations rise slightly until 2040 and decrease in the second half of the century, when a small drop in the size of large ozone episodes is found. This suggests that the fate of future European ozone episodes will be controlled not only by regional emissions but also by the evolution of global emissions of methane (Fortems-Cheiney et al., 2017; Abernethy et al., 2021; Allen et al., 2021; Liu et al., 2022b), which has low reactivity and therefore persists in the troposphere much longer than other precursors (~10 years).

The growth in the size of the ozone episodes in the high forcing scenarios (ssp370 and ssp585) appears to be related to both rising temperatures and upward trends in the emissions of some precursors. While CO, anthropogenic NMVOCs and NO_x emissions remain at similar levels to those in the last years of the historical period, there are more prominent changes in total VOC emissions and methane concentrations for these scenarios. The ssp585 scenario features strong interannual variability in the size of the episodes as well as some decreases in the last two decades of the century. The latter roughly coincide with the time when both methane and NO_x begin to decline but might also be affected by interannual variability. On the other hand, ssp370 is the only simulation for which both methane concentrations and large ozone episodes increase until the end of the century, pointing again at the need to control both regional and global emissions of CH_4. The larger sizes of episodes in ssp585 compared to ssp370 until at least 2080, despite lower methane concentrations, may be due to the higher temperatures and NO_x emissions in the former. Understanding these differences as well as the strong interannual variability of ozone episodes in ssp585– probably related to changes in meteorology – requires further investigations that are beyond the scope of this study.

5. Summary and conclusion

A novel pseudo-Lagrangian algorithm has been developed to track large-scale ozone episodes by connecting local extremes (exceedances of local 95th percentiles of daily O_3 maxima in April–September of a given reference period) extending over space and time for at least three days. The algorithm has been applied to examine changes in European ozone episodes in the CAMS reanalysis (2003–2022) as well as in the historical simulation (1950–2014) and future projections (2015–2100; scenarios ssp126, ssp245, ssp370, and ssp585) simulated by UKESM1 as part of CMIP6. Episodes have been characterized according to their areal extent.

An analysis of the 100 largest episodes in CAMS reveals that they have mainly occurred in central or southern Europe in June–September (60 episodes with mean latitude south of 50° N) and in northern Europe in April–May (27 episodes north of 50° N). While the total number of episodes per year have increased after 2015, probably associated with the occurrence of elevated summer and spring temperatures, the annual frequency of the 100 largest ozone episodes has decreased. Eight out of the top ten episodes occurred from 2003 to 2007, with the two remaining in 2010 and 2013, in all cases associated with heatwave conditions. The decrease in large ozone episodes can be attributed to the control of precursor emissions over the last 20 years, even though high spring-summer temperatures have been recorded in recent years such as 2018 and 2022. These findings support the effectiveness of European air quality strategies to reduce peak ozone concentrations, as also reported by previous studies (e.g., Paoletti et al., 2014; Boleti et al., 2020; Otero et al., 2021; Zohdirad et al., 2022).

Despite the results found for CAMS, there are considerable uncertainties in the size of European ozone episodes over the rest of the century according to UKESM1 climate projections. The clear trend toward smaller episodes observed in recent years would continue in the future only for the scenario with stronger precursor emission decreases and temperature controls (ssp126). This situation could be reversed, especially under the most extreme climate change scenarios (ssp370 and ssp585). In such scenarios, the combined effects of climate change (rising temperatures and probably changes to stagnation events, e.g., Horton et al., 2012, 2014) and precursor changes (enhanced atmospheric concentrations of CH_4 and NMVOC emissions, while regional NO_x and CO emissions remain hardly unchanged) may deteriorate the ozone pollution problem to levels not even found in the years before the implementation of European air pollution policies. Future measures targeting global concentrations of CH_4 can be beneficial to control both near-term warming and ozone episodes, as indicated by previous assessments of the co-benefits of climate and air quality policies (Turnock et al., 2022, and references therein). Nevertheless, understanding the reasons for the uneven results found for the different projections, although seemingly related to emission and temperature changes, is complicated by the effect of climate variability, which seems to be particularly strong for the high forcing scenarios (ssp585 and, to a lesser extent, ssp370). Further research is therefore needed, including the assessment of ozone episodes in dedicated model experiments and ensembles of different climate models (Doherty et al., 2022; Fiore et al., 2022).

In future work, we will examine atmosphere-only experiments of UKESM1 with different forcings (e.g., Collins et al., 2017; Turnock et al., 2022; Zanis et al., 2022). This will enable quantifying the separate effects of climate change and emissions of the different precursors on the evolution of future ozone episodes, and understanding whether there is a limit to the benefits of regional emission reductions in a warming climate. In addition, we will assess the separate role of the atmospheric circulation, rising atmospheric temperatures and drying soils in the interannual fluctuations of the largest episodes. Furthermore, the algorithm presented in this work can be adapted to other air pollutants, and applied to track the origins of air pollution episodes in other regions of the world which are vulnerable to climate change and face emerging air quality problems.

Understanding the drivers of such episodes under a changing climate will be crucial to issue efficient air quality policies that attack the root of the problem with moderate socio-economic and health costs to society.

CRediT authorship contribution statement

Rodrigo Crespo-Miguel: Formal analysis, Visualization, Writing – Original Draft. **Carlos Ordóñez:** Methodology, Supervision, Project administration, Funding acquisition, Writing – Review and Editing. **Ricardo García-Herrera:** Supervision, Project administration, Funding acquisition, Writing – Review and Editing. **Jordan L. Schnell:** Software, Writing - Review and Editing. **Steven T. Turnock:** Writing - Review and Editing.

Declaration of competing interest

The authors declare that they have no known competing financial interests or personal relationships that could have appeared to influence the work reported in this paper.

Data availability

Reanalysis and UKESM1 data used in this work are publicly available. The observational ozone dataset can be made available on request.

Acknowledgements

We acknowledge support from MALONE (PID2021-122252OB-I00), project funded by MICIU/AEI/10.13039/501100011033 and ERDF, EU. This research was supported in part by the NOAA cooperative agreement NA22OAR4320151, for the Cooperative Institute for Earth System Research and Data Science (CIESRDS). The statements, findings, conclusions, and recommendations are those of the author(s) and do not necessarily reflect the views of NOAA or the U.S. Department of Commerce.

References

Abernethy, S., O’Connor, F. M., Jones, C. D., and Jackson, R. B.: Methane removal and the proportional reductions in surface temperature and ozone, Philosophical Transactions of the Royal Society A: Mathematical, Physical and Engineering Sciences, 379, https://doi.org/10.1098/rsta.2021.0104, 2021.

Aggelis, D., Zanis, P., Zerefos, C. S., Bais, A. F., and Nastos, P. T.: Mapping of surface ozone seasonality and trends across Europe during 1997-2006 through kriging interpolation to observational data, Water Air Soil Pollut, 224, https://doi.org/10.1007/s11270-013-1501-9, 2013.

Allen, R. J., Horowitz, L. W., Naik, V., Oshima, N., O’Connor, F. M., Turnock, S., Shim, S., Le Sager, P., Van Noije, T., Tsigaridis, K., Bauer, S. E., Sentman, L. T., John, J. G., Broderick, C., Deushi, M., Folberth, G. A., Fujimori, S., and Collins, W. J.: Significant climate benefits from near-term climate forcer mitigation in spite of aerosol reductions, Environmental Research Letters, 16, https://doi.org/10.1088/1748-9326/abe06b, 2021.

Archibald, A. T., Ordóñez, C., Brent, E., and Williams, M. L.: Potential impacts of emissions associated with unconventional hydrocarbon extraction on UK air quality and human health, Air Qual Atmos Health, 11, https://doi.org/10.1007/s11869-018-0570-8, 2018.

Archibald, A. T., O’Connor, F. M., Abraham, N. L., Archer-Nicholls, S., Chipperfield, M. P., Dalvi, M., Folberth, G. A., Dennison, F., Dhomse, S. S., Griffiths, P. T., Hardacre, C., Hewitt, A. J., Hill, R. S., Johnson, C. E., Keeble, J., Köhler, M. O., Morgenstern, O., Mulcahy, J. P., Ordóñez, C., Pope, R. J., Rumbold, S. T., Russo, M. R., Savage, N. H., Sellar, A., Stringer, M., Turnock, S. T., Wild, O., and Zeng, G.: Description and evaluation of the UKCA stratosphere-troposphere chemistry scheme (StratTrop vn 1.0) implemented in UKESM1, Geosci Model Dev, 13, https://doi.org/10.5194/gmd-13-1223-2020, 2020a.

Archibald, A. T., Turnock, S. T., Griffiths, P. T., Cox, T., Derwent, R. G., Knote, C., and Shin, M.: On the changes in surface ozone over the twenty-first century: sensitivity to changes in surface temperature and chemical mechanisms: 21st century changes in surface ozone, Philosophical Transactions of the Royal Society A: Mathematical, Physical and Engineering Sciences, 378, https://doi.org/10.1098/rsta.2019.0329, 2020b.

Ashmore, M. R.: Assessing the future global impacts of ozone on vegetation, https://doi.org/10.1111/j.1365-3040.2005.01341.x, 2005.

Atkinson, R.: Atmospheric chemistry of VOCs and NOx, Atmos Environ, 34, 2000.

Ballester, J., Quijal-Zamorano, M., Méndez Turrubiates, R. F., Pegenaute, F., Herrmann, F. R., Robine, J. M., Basagaña, X., Tonne, C., Antó, J. M., and Achebak, H.: Heat-related mortality in Europe during the summer of 2022, Nat Med, 29, https://doi.org/10.1038/s41591-023-02419-z, 2023.

Barriopedro, D., Fischer, E. M., Luterbacher, J., Trigo, R. M., and García-Herrera, R.: The hot summer of 2010: Redrawing the temperature record map of Europe, Science (1979), 332, https://doi.org/10.1126/science.1201224, 2011.

Barriopedro, D., Sousa, P. M., Trigo, R. M., García-Herrera, R., and Ramos, A. M.: The exceptional Iberian heatwave of summer 2018, https://doi.org/10.1175/BAMS-D-19-0159.1, 2020.

Barriopedro, D., García-Herrera, R., Ordóñez, C., Miralles, D. G., and Salcedo-Sanz, S.: Heat Waves: Physical Understanding and Scientific Challenges, Reviews of Geophysics, 61, https://doi.org/10.1029/2022RG000780, 2023.

Bloomer, B. J., Stehr, J. W., Piety, C. A., Salawitch, R. J., and Dickerson, R. R.: Observed relationships of ozone air pollution with temperature and emissions, Geophys Res Lett, 36, https://doi.org/10.1029/2009GL037308, 2009.

Boleti, E., Hueglin, C., and Takahama, S.: Ozone time scale decomposition and trend assessment from surface observations in Switzerland, Atmos Environ, 191, https://doi.org/10.1016/j.atmosenv.2018.07.039, 2018.

Boleti, E., Hueglin, C., K. Grange, S., and Takahama, S.: Temporal and spatial analysis of ozone concentrations in Europe based on timescale decomposition and a multi-clustering approach, Atmos Chem Phys, 20, https://doi.org/10.5194/acp-20-9051-2020, 2020.

Carro-Calvo, L., Ordóñez, C., García-Herrera, R., and Schnell, J. L.: Spatial clustering and meteorological drivers of summer ozone in Europe, Atmos Environ, 167, https://doi.org/10.1016/j.atmosenv.2017.08.050, 2017.

Chen, Z.-Y., Petetin, H., Méndez Turrubiates, R. F., Achebak, H., Pérez García-Pando, C., and Ballester, J.: Population exposure to multiple air pollutants and its compound episodes in Europe, Nat Commun, 15, 2094, https://doi.org/10.1038/s41467-024-46103-3, 2024.

Climate Action Network Europe: This is Climate Change in Europe, https://caneurope.org/content/uploads/2013/11/CANEurope-EUImpactsReport2013_final.pdf, 2013.

Colette, A., Andersson, C., Baklanov, A., Bessagnet, B., Brandt, J., Christensen, J. H., Doherty, R., Engardt, M., Geels, C., Giannakopoulos, C., Hedegaard, G. B., Katragkou, E., Langner, J., Lei, H., Manders, A., Melas, D., Meleux, F., Rouïl, L., Sofiev, M., Soares, J., Stevenson, D. S., Tombrou-Tzella, M., Varotsos, K. V., and Young, P.: Is the ozone climate penalty robust in Europe?, Environmental Research Letters, 10, https://doi.org/10.1088/1748-9326/10/8/084015, 2015.

Colette, A., Andersson, C., Manders, A., Mar, K., Mircea, M., Pay, M. T., Raffort, V., Tsyro, S., Cuvelier, C., Adani, M., Bessagnet, B., Bergström, R., Briganti, G., Butler, T., Cappelletti, A., Couvidat, F., D'Isidoro, M., Doumbia, T., Fagerli, H., Granier, C., Heyes, C., Klimont, Z., Ojha, N., Otero, N., Schaap, M., Sindelarova, K., Stegehuis, A. I., Roustan, Y., Vautard, R., Van Meijgaard, E., Garcia Vivanco, M., and Wind, P.: EURODELTA-Trends, a multi-model experiment of air quality hindcast in Europe over 1990-2010, Geosci Model Dev, 10, https://doi.org/10.5194/gmd-10-3255-2017, 2017.

Collins, J. W., Lamarque, J. F., Schulz, M., Boucher, O., Eyring, V., Hegglin, I. M., Maycock, A., Myhre, G., Prather, M., Shindell, D., and Smith, J. S.: AerChemMIP: Quantifying the effects of chemistry and aerosols in CMIP6, Geosci Model Dev, 10, https://doi.org/10.5194/gmd-10-585-2017, 2017.

Copernicus: European temperature, https://climate.copernicus.eu/european-temperature, 2018. Last access on 26th April 2024.

Copernicus: Summer 2022 Europe's hottest on record, https://climate.copernicus.eu/copernicus-summer-2022-europes-hottest-record, 2022. Last access on 26th April 2024.

Curriero, F. C., Heiner, K. S., Samet, J. M., Zeger, S. L., Strug, L., and Patz, J. A.: Temperature and mortality in 11 cities of the eastern United States, Am J Epidemiol, 155, https://doi.org/10.1093/aje/155.1.80, 2002.

Derwent, R. G. and Parrish, D. D.: Analysis and assessment of the observed long-term changes over three decades in ground-level ozone across north-west Europe from 1989 - 2018, Atmos Environ, 286, https://doi.org/10.1016/j.atmosenv.2022.119222, 2022.

Derwent, R. G., Parrish, D. D., Manning, A. J., Spain, T. G., Simmonds, P. G., and O'Doherty, S.: Ozone at Mace Head, Ireland from 1987 to 2021: Declining baselines, phase-out of European regional pollution, COVID-19 impacts, Atmos Environ, 320, 120322, https://doi.org/10.1016/j.atmosenv.2023.120322, 2024.

Doherty, R. M., O'Connor, F. M., and Turnock, S. T.: Projections of Future Air Quality Are Uncertain. But Which Source of Uncertainty Is Most Important?, https://doi.org/10.1029/2022JD037948, 2022.

European Environment Agency (EEA): Air quality in Europe – 2020 report. Luxembourg, Publications Office of the European Union, 2020. https://data.europa.eu/doi/10.2800/786656.

EMEP/CCC-Report 1/2016: Air pollution trends in the EMEP region between 1990 and 2012, Norwegian Institute of Air Research, Kjeller, Norway, https://unece.org/info/publications/pub/21555, 2016.

European Commission: Directive 2008/50/EC of the European Parliament and of the Council of 21 May 2008 on ambient air quality and cleaner air for Europe, Official Journal of the European Union, 152, 2008.

Fenech, S., Doherty, R. M., Heaviside, C., Vardoulakis, S., Macintyre, H. L., and O'Connor, F. M.: The influence of model spatial resolution on simulated ozone and fine particulate matter for Europe: Implications for health impact assessments, Atmos Chem Phys, 18, https://doi.org/10.5194/acp-18-5765-2018, 2018.

Feng, Z., Büker, P., Pleijel, H., Emberson, L., Karlsson, P. E., and Uddling, J.: A unifying explanation for variation in ozone sensitivity among woody plants, Glob Chang Biol, 24, https://doi.org/10.1111/gcb.13824, 2018.

Fiore, A. M., Naik, V., Spracklen, D. V., Steiner, A., Unger, N., Prather, M., Bergmann, D., Cameron-Smith, P. J., Cionni, I., Collins, W. J., Dalsøren, S., Eyring, V., Folberth, G. A., Ginoux, P., Horowitz, L. W., Josse, B., Lamarque, J.-F., MacKenzie, I. A., Nagashima, T., O'Connor, F. M., Righi, M., Rumbold, S. T., Shindell, D. T., Skeie, R. B., Sudo, K., Szopa, S., Takemura, T., and Zeng, G.: Global air quality and climate, Chem Soc Rev, 41, 6663, https://doi.org/10.1039/c2cs35095e, 2012.

Fiore, A. M., Milly, G. P., Hancock, S. E., Quiñones, L., Bowden, J. H., Helstrom, E., Lamarque, J. F., Schnell, J., West, J. J., and Xu, Y.: Characterizing Changes in Eastern U.S. Pollution Events in a Warming World, Journal of Geophysical Research: Atmospheres, 127, https://doi.org/10.1029/2021JD035985, 2022.

Flemming, J., Huijnen, V., Arteta, J., Bechtold, P., Beljaars, A., Blechschmidt, A. M., Diamantakis, M., Engelen, R. J., Gaudel, A., Inness, A., Jones, L., Josse, B., Katragkou, E., Marecal, V., Peuch, V. H., Richter, A., Schultz, M. G., Stein, O., and Tsikerdekis, A.: Tropospheric chemistry in the integrated forecasting system of ECMWF, Geosci Model Dev, 8, https://doi.org/10.5194/gmd-8-975-2015, 2015.

Fortems-Cheiney, A., Foret, G., Siour, G., Vautard, R., Szopa, S., Dufour, G., Colette, A., Lacressonniere, G., and Beekmann, M.: A 3 °C global RCP8.5 emission trajectory cancels benefits of European emission reductions on air quality, Nat Commun, 8, https://doi.org/10.1038/s41467-017-00075-9, 2017.

Founda, D. and Giannakopoulos, C.: The exceptionally hot summer of 2007 in Athens, Greece - A typical summer in the future climate?, Glob Planet Change, 67, https://doi.org/10.1016/j.gloplacha.2009.03.013, 2009.

Fu, T. M. and Tian, H.: Climate Change Penalty to Ozone Air Quality: Review of Current Understandings and Knowledge Gaps, https://doi.org/10.1007/s40726-019-00115-6, 2019.

Garcia-Herrera, R., Díaz, J., Trigo, R. M., Luterbacher, J., and Fischer, E. M.: A review of the european summer heat wave of 2003, https://doi.org/10.1080/10643380802238137, 2010.

Garrido-Perez, J. M., Ordóñez, C., García-Herrera, R., and Schnell, J. L.: The differing impact of air stagnation on summer ozone across Europe, Atmos Environ, 219, https://doi.org/10.1016/j.atmosenv.2019.117062, 2019.

GBD 2019 Risk Factors Collaborators: Global burden of 87 risk factors in 204 countries and territories, 1990–2019: a systematic analysis for the Global Burden of Disease Study 2019, The Lancet, 396, 1223–1249, https://doi.org/10.1016/S0140-6736(20)30752-2, 2020.

Gu, Y., Henze, D. K., Nawaz, M. O., and Wagner, U. J.: Response of the ozone-related health burden in Europe to changes in local anthropogenic emissions of ozone precursors, Environmental Research Letters, 18, 114034, https://doi.org/10.1088/1748-9326/ad0167, 2023.

Hall, J. and Loboda, T.: Quantifying the variability of potential black carbon transport from cropland burning in Russia driven by atmospheric blocking events, Environmental Research Letters, 13, https://doi.org/10.1088/1748-9326/aabf65, 2018.

Hersbach, H., Bell, B., Berrisford, P., Hirahara, S., Horányi, A., Muñoz-Sabater, J., Nicolas, J., Peubey, C., Radu, R., Schepers, D., Simmons, A., Soci, C., Abdalla, S., Abellan, X., Balsamo, G., Bechtold, P., Biavati, G., Bidlot, J., Bonavita, M., De Chiara, G., Dahlgren, P., Dee, D., Diamantakis, M., Dragani, R., Flemming, J., Forbes, R., Fuentes, M., Geer, A., Haimberger, L., Healy, S., Hogan, R. J., Hólm, E., Janisková, M., Keeley, S., Laloyaux, P., Lopez, P., Lupu, C., Radnoti, G., de Rosnay, P., Rozum, I., Vamborg, F., Villaume, S., and Thépaut, J. N.: The ERA5 global reanalysis, Quarterly Journal of the Royal Meteorological Society, 146, https://doi.org/10.1002/qj.3803, 2020.

Horstman, D., McDonnell, V., Folinsbbe, L., Abdul-Salaam, S., and Ives, P.: Changes in pulmonary function and airway reactivity due to prolonged exposure to typical ambient ozone (O 3) levels, in: Studies in Environmental Science, https://doi.org/10.1016/S0166-1116(08)70639-3, 1989.

Horton, D. E., Harshvardhan, and Diffenbaugh, N. S.: Response of air stagnation frequency to anthropogenically enhanced radiative forcing, Environmental Research Letters, 7, https://doi.org/10.1088/1748-9326/7/4/044034, 2012.

Horton, D. E., Skinner, C. B., Singh, D., and Diffenbaugh, N. S.: Occurrence and persistence of future atmospheric stagnation events, Nat Clim Chang, 4, https://doi.org/10.1038/nclimate2272, 2014.

Huijnen, V., Le Sager, P., Köhler, M. O., Carver, G., Rémy, S., Flemming, J., Chabrillat, S., Errera, Q., and Van Noije, T.: OpenIFS/AC: atmospheric chemistry and aerosol in OpenIFS 43r3, Geosci Model Dev, 15, https://doi.org/10.5194/gmd-15-6221-2022, 2022.

Inness, A., Ades, M., Agustí-Panareda, A., Barr, J., Benedictow, A., Blechschmidt, A. M., Jose Dominguez, J., Engelen, R., Eskes, H., Flemming, J., Huijnen, V., Jones, L., Kipling, Z., Massart, S., Parrington, M., Peuch, V. H., Razinger, M., Remy, S., Schulz, M., and Suttie, M.: The CAMS reanalysis of atmospheric composition, Atmos Chem Phys, 19, https://doi.org/10.5194/acp-19-3515-2019, 2019.

Jacob, D. J. and Winner, D. A.: Effect of climate change on air quality, Atmos Environ, 43, https://doi.org/10.1016/j.atmosenv.2008.09.051, 2009.

Karlsson, P. E., Klingberg, J., Engardt, M., Andersson, C., Langner, J., Karlsson, G. P., and Pleijel, H.: Past, present and future concentrations of ground-level ozone and potential impacts on ecosystems and human health in northern Europe, https://doi.org/10.1016/j.scitotenv.2016.10.061, 2017.

Kerr, G. H., Waugh, D. W., Strode, S. A., Steenrod, S. D., Oman, L. D., and Strahan, S. E.: Disentangling the Drivers of the Summertime Ozone-Temperature Relationship Over the United States, Journal of Geophysical Research: Atmospheres, 124, https://doi.org/10.1029/2019JD030572, 2019.

Kleinman, L. I., Daum, P. H., Lee, Y. N., Nunnermácker, L. J., Springston, S. R., Weinstein-Lloyd, J., and Rudolph, J.: Ozone production efficiency in an urban area, Journal of Geophysical Research Atmospheres, 107, https://doi.org/10.1029/2002JD002529, 2002.

Konovalov, I. B., Beekmann, M., Kuznetsova, I. N., Yurova, A., and Zvyagintsev, A. M.: Atmospheric impacts of the 2010 Russian wildfires: Integrating modelling and measurements of an extreme air pollution episode in the Moscow region, Atmos Chem Phys, 11, https://doi.org/10.5194/acp-11-10031-2011, 2011.

Kovats, R. S. and Hajat, S.: Heat stress and public health: A critical review, in: Annual Review of Public Health, https://doi.org/10.1146/annurev.publhealth.29.020907.090843, 2008.

Lass, W., Haas, A., Hinkel, J., and Jaeger, C.: Avoiding the avoidable: Towards a European heat waves risk governance, International Journal of Disaster Risk Science, 2, https://doi.org/10.1007/s13753-011-0001-z, 2011.

Leibensperger, E. M., Mickley, L. J., and Jacob, D. J.: Sensitivity of US air quality to mid-latitude cyclone frequency and implications of 1980-2006 climate change, Atmos Chem Phys, 8, https://doi.org/10.5194/acp-8-7075-2008, 2008.

Lian, Z., Qi, H., Liu, X., Zhang, Y., Xu, R., Yang, X., Zeng, Y., and Li, J.: Ambient ozone, and urban PM2.5 co-exposure, aggravate allergic asthma via transient receptor potential vanilloid 1-mediated neurogenic inflammation, Ecotoxicol Environ Saf, 243, https://doi.org/10.1016/j.ecoenv.2022.114000, 2022.

Liu, H., Liu, S., Xue, B., Lv, Z., Meng, Z., Yang, X., Xue, T., Yu, Q., and He, K.: Ground-level ozone pollution and its health impacts in China, Atmos Environ, 173, https://doi.org/10.1016/j.atmosenv.2017.11.014, 2018.

Liu, Z., Doherty, R. M., Wild, O., O'connor, F. M., and Turnock, S. T.: Correcting ozone biases in a global chemistry-climate model: implications for future ozone, Atmos Chem Phys, 22, https://doi.org/10.5194/acp-22-12543-2022, 2022a.

Liu, Z., Doherty, R. M., Wild, O., O'connor, F. M., and Turnock, S. T.: Tropospheric ozone changes and ozone sensitivity from the present day to the future under shared socioeconomic pathways, Atmos Chem Phys, 22, https://doi.org/10.5194/acp-22-1209-2022, 2022b.

Lupaşcu, A. and Butler, T.: Source attribution of European surface O3 using a tagged O3 mechanism, Atmos Chem Phys, 19, https://doi.org/10.5194/acp-19-14535-2019, 2019.

Lyapina, O., Schultz, M. G., and Hense, A.: Cluster analysis of European surface ozone observations for evaluation of MACC reanalysis data, Atmos Chem Phys, 16, https://doi.org/10.5194/acp-16-6863-2016, 2016.

Markakis, K., Valari, M., Engardt, M., Lacressonniere, G., Vautard, R., and Andersson, C.: Mid-21st century air quality at the urban scale under the influence of changed climate and emissions-case studies for Paris and Stockholm, Atmos Chem Phys, 16, https://doi.org/10.5194/acp-16-1877-2016, 2016.

McMichael, A. J., Woodruff, R. E., and Hales, S.: Climate change and human health: Present and future risks, https://doi.org/10.1016/S0140-6736(06)68079-3, 2006.

Monks, P. S.: A review of the observations and origins of the spring ozone maximum, Atmos Environ, 34, https://doi.org/10.1016/S1352-2310(00)00129-1, 2000.

Monks, P. S., Archibald, A. T., Colette, A., Cooper, O., Coyle, M., Derwent, R., Fowler, D., Granier, C., Law, K. S., Mills, G. E., Stevenson, D. S., Tarasova, O., Thouret, V., Von Schneidemesser, E., Sommariva, R., Wild, O., and Williams, M. L.: Tropospheric ozone and its precursors from the urban to the global scale from air quality to short-lived climate forcer, https://doi.org/10.5194/acp-15-8889-2015, 2015.

NOAA: Monthly Global Climate Report for May 2013, 2013.

Oltmans, S. J.: Surface ozone measurements in clean air., J Geophys Res, 86, https://doi.org/10.1029/JC086iC02p01174, 1981.

Ordóñez, C., Mathis, H., Furger, M., Henne, S., Hüglin, C., Staehelin, J., and Prévŏt, A. S. H.: Changes of daily surface ozone maxima in Switzerland in all seasons from 1992 to 2002 and discussion of summer 2003, Atmos Chem Phys, 5, https://doi.org/10.5194/acp-5-1187-2005, 2005.

Ordóñez, C., Elguindi, N., Stein, O., Huijnen, V., Flemming, J., Inness, A., Flentje, H., Katragkou, E., Moinat, P., Peuch, V. H., Segers, A., Thouret, V., Athier, G., Van Weele, M., Zerefos, C. S., Cammas, J. P., and Schultz, M. G.: Global model simulations of air pollution during the 2003 European heat wave, Atmos Chem Phys, 10, https://doi.org/10.5194/acp-10-789-2010, 2010.

Ordóñez, C., Garrido-Perez, J. M., and García-Herrera, R.: Early spring near-surface ozone in Europe during the COVID-19 shutdown: Meteorological effects outweigh emission changes, Science of the Total Environment, 747, https://doi.org/10.1016/j.scitotenv.2020.141322, 2020.

Orru, H., Andersson, C., Ebi, K. L., Langner, J., Åström, C., and Forsberg, B.: Impact of climate change on ozone-related mortality and morbidity in Europe, European Respiratory Journal, 41, https://doi.org/10.1183/09031936.00210411, 2013.

Orru, H., Åström, C., Andersson, C., Tamm, T., Ebi, K. L., and Forsberg, B.: Ozone and heat-related mortality in Europe in 2050 significantly affected by changes in climate, population and greenhouse gas emission, Environmental Research Letters, 14, https://doi.org/10.1088/1748-9326/ab1cd9, 2019.

Otero, N., Sillmann, J., Schnell, J. L., Rust, H. W., and Butler, T.: Synoptic and meteorological drivers of extreme ozone concentrations over Europe, Environ. Res. Lett, 11, 2016.

Otero, N., Rust, H. W., and Butler, T.: Temperature dependence of tropospheric ozone under NOx reductions over Germany, Atmos Environ, 253, https://doi.org/10.1016/j.atmosenv.2021.118334, 2021.

Otero, N., Jurado, O. E., Butler, T., and Rust, H. W.: The impact of atmospheric blocking on the compounding effect of ozone pollution and temperature: A copula-based approach, Atmos Chem Phys, 22, https://doi.org/10.5194/acp-22-1905-2022, 2022.

Paoletti, E., De Marco, A., Beddows, D. C. S., Harrison, R. M., and Manning, W. J.: Ozone levels in European and USA cities are increasing more than at rural sites, while peak values are decreasing, Environmental Pollution, 192, https://doi.org/10.1016/j.envpol.2014.04.040, 2014.

Penkett, S. A. and Brice, K. A.: The spring maximum in photo-oxidants in the Northern Hemisphere troposphere, Nature, 319, https://doi.org/10.1038/319655a0, 1986.

Pope, R. J., Kerridge, B. J., Chipperfield, M. P., Siddans, R., Latter, B. G., Ventress, L. J., Pimlott, M. A., Feng, W., Comyn-Platt, E., Hayman, G. D., Arnold, S. R., and Graham, A. M.: Investigation of the summer 2018 European ozone air pollution episodes using novel satellite data and modelling, Atmos Chem Phys, 23, 13235–13253, https://doi.org/10.5194/acp-23-13235-2023, 2023.

Porter, W. C. and Heald, C. L.: The mechanisms and meteorological drivers of the summertime ozone-temperature relationship, Atmos Chem Phys, 19, https://doi.org/10.5194/acp-19-13367-2019, 2019.

Rasmussen, D. J., Hu, J., Mahmud, A., and Kleeman, M. J.: The ozone-climate penalty: Past, present, and future, Environ Sci Technol, 47, https://doi.org/10.1021/es403446m, 2013.

Real, E., Megaritis, A., Colette, A., Valastro, G., and Messina, P.: Atlas of ozone chemical regimes in Europe, Atmos Environ, 320, 120323, https://doi.org/10.1016/j.atmosenv.2023.120323, 2024.

Rebetez, M., Dupont, O., and Giroud, M.: An analysis of the July 2006 heatwave extent in Europe compared to the record year of 2003, Theor Appl Climatol, 95, https://doi.org/10.1007/s00704-007-0370-9, 2009.

Rousi, E., Fink, A. H., Andersen, L. S., Becker, F. N., Beobide-Arsuaga, G., Breil, M., Cozzi, G., Heinke, J., Jach, L., Niermann, D., Petrovic, D., Richling, A., Riebold, J., Steidl, S., Suarez-Gutierrez, L., Tradowsky, J. S., Coumou, D., Düsterhus, A., Ellsäßer, F., Fragkoulidis, G., Gliksman, D., Handorf, D., Haustein, K., Kornhuber, K., Kunstmann, H., Pinto, J. G., Warrach-Sagi, K., and Xoplaki, E.: The extremely hot and dry 2018 summer in central and northern Europe from a multi-faceted weather and climate perspective, Natural Hazards and Earth System Sciences, 23, https://doi.org/10.5194/nhess-23-1699-2023, 2023.

Russo, S., Sillmann, J., and Fischer, E. M.: Top ten European heatwaves since 1950 and their occurrence in the coming decades, Environmental Research Letters, 10, https://doi.org/10.1088/1748-9326/10/12/124003, 2015.

Sánchez-Benítez, A., Barriopedro, D., and García-Herrera, R.: Tracking Iberian heatwaves from a new perspective, Weather Clim Extrem, 28, https://doi.org/10.1016/j.wace.2019.100238, 2020.

Sarwar, G., Hogrefe, C., Henderson, B. H., Mathur, R., Gilliam, R., Callaghan, A. B., Lee, J., and Carpenter, L. J.: Impact of particulate nitrate photolysis on air quality over the Northern Hemisphere, Science of the Total Environment, 917, https://doi.org/10.1016/j.scitotenv.2024.170406, 2024.

Scheel, H. E., Areskoug, H., Geiß, H., Gomiscek, B., Granby, K., Haszpra, L., Klasinc, L., Kley, D., Laurila, T., Lindskog, A., Roemer, M., Schmitt, R., Simmonds, P., Solberg, S., and Toupance, G.: On the spatial distribution and seasonal variation of lower-troposphere ozone over Europe, in: Journal of Atmospheric Chemistry, https://doi.org/10.1023/A:1005882922435, 1997.

Schnell, J. L., Holmes, C. D., Jangam, A., and Prather, M. J.: Skill in forecasting extreme ozone pollution episodes with a global atmospheric chemistry model, Atmos Chem Phys, 14, https://doi.org/10.5194/acp-14-7721-2014, 2014.

Schnell, J. L., Prather, M. J., Josse, B., Naik, V., Horowitz, L. W., Cameron-Smith, P., Bergmann, D., Zeng, G., Plummer, D. A., Sudo, K., Nagashima, T., Shindell, D. T., Faluvegi, G., and Strode, S. A.: Use of North American and European air quality networks to evaluate global chemistry-climate modeling of surface ozone, Atmos Chem Phys, 15, https://doi.org/10.5194/acp-15-10581-2015, 2015.

Sellar, A. A., Jones, C. G., Mulcahy, J. P., Tang, Y., Yool, A., Wiltshire, A., O'Connor, F. M., Stringer, M., Hill, R., Palmieri, J., Woodward, S., de Mora, L., Kuhlbrodt, T., Rumbold, S. T., Kelley, D. I., Ellis, R., Johnson, C. E., Walton, J., Abraham, N. L., Andrews, M. B., Andrews, T., Archibald, A. T., Berthou, S., Burke, E., Blockley, E., Carslaw, K., Dalvi, M., Edwards, J., Folberth, G. A., Gedney, N., Griffiths, P. T., Harper, A. B., Hendry, M. A., Hewitt, A. J., Johnson, B., Jones, A., Jones, C. D., Keeble, J., Liddicoat, S., Morgenstern, O., Parker, R. J., Predoi, V., Robertson, E., Siahaan, A., Smith, R. S., Swaminathan, R., Woodhouse, M. T., Zeng, G., and Zerroukat, M.: UKESM1: Description and Evaluation of the U.K. Earth System Model, J Adv Model Earth Syst, 11, https://doi.org/10.1029/2019MS001739, 2019.

Sicard, P., De Marco, A., Troussier, F., Renou, C., Vas, N., and Paoletti, E.: Decrease in surface ozone concentrations at Mediterranean remote sites and increase in the cities, Atmos Environ, 79, https://doi.org/10.1016/j.atmosenv.2013.07.042, 2013.

Sicard, P., De Marco, A., Agathokleous, E., Feng, Z., Xu, X., Paoletti, E., Rodriguez, J. J. D., and Calatayud, V.: Amplified ozone pollution in cities during the COVID-19 lockdown, Science of the Total Environment, 735, https://doi.org/10.1016/j.scitotenv.2020.139542, 2020.

Sillman, S.: The relation between ozone, NOx and hydrocarbons in urban and polluted rural environments, Atmos Environ, 33, 1821–1845, https://doi.org/10.1016/S1352-2310(98)00345-8, 1999.

Solberg, S., Derwent, R. G., Hov, Ø., Langner, J., and Lindskog, A.: European abatement of surface ozone in a global perspective, https://doi.org/10.1579/0044-7447-34.1.47, 2005.

Solberg, S., Hov, Søvde, A., Isaksen, I. S. A., Coddeville, P., De Backer, H., Forster, C., Orsolini, Y., and Uhse, K.: European surface ozone in the extreme summer 2003, Journal of Geophysical Research Atmospheres, 113, https://doi.org/10.1029/2007JD009098, 2008.

Sousa, P. M., Barriopedro, D., García-Herrera, R., Ordóñez, C., Soares, P. M. M., and Trigo, R. M.: Distinct influences of large-scale circulation and regional feedbacks in two exceptional 2019 European heatwaves, Commun Earth Environ, 1, https://doi.org/10.1038/s43247-020-00048-9, 2020.

Stevenson, D. S., Dentener, F. J., Schultz, M. G., Ellingsen, K., van Noije, T. P. C., Wild, O., Zeng, G., Amann, M., Atherton, C. S., Bell, N., Bergmann, D. J., Bey, I., Butler, T., Cofala, J., Collins, W. J., Derwent, R. G., Doherty, R. M., Drevet, J., Eskes, H. J., Fiore, A. M., Gauss, M., Hauglustaine, D. A., Horowitz, L. W., Isaksen, I. S. A., Krol, M. C., Lamarque, J. F., Lawrence, M. G., Montanaro, V., Müller, J. F., Pitari, G., Prather, M. J., Pyle, J. A., Rast, S., Rodriquez, J. M., Sanderson, M. G., Savage, N. H., Shindell, D. T., Strahan, S. E., Sudo, K., and Szopa, S.: Multimodel ensemble simulations of present-day and near-future tropospheric ozone, Journal of Geophysical Research Atmospheres, 111, https://doi.org/10.1029/2005JD006338, 2006.

Stohl, A., Berg, T., Burkhart, J. F., Fjæraa, A. M., Forster, C., Herber, A., Hov, Lunder, C., McMillan, W. W., Oltmans, S., Shiobara, M., Simpson, D., Solberg, S., Stebel, K., Ström, J., Tørseth, K., Treffeisen, R., Virkkunen, K., and Yttri, K. E.: Arctic smoke - Record high air pollution levels in the European Arctic due to agricultural fires in Eastern Europe in spring 2006, Atmos Chem Phys, 7, https://doi.org/10.5194/acp-7-511-2007, 2007.

Tai, A. P. K. and Val Martin, M.: Impacts of ozone air pollution and temperature extremes on crop yields: Spatial variability, adaptation and implications for future food security, Atmos Environ, 169, https://doi.org/10.1016/j.atmosenv.2017.09.002, 2017.

Tai, A. P. K., Martin, M. V., and Heald, C. L.: Threat to future global food security from climate change and ozone air pollution, Nat Clim Chang, 4, https://doi.org/10.1038/nclimate2317, 2014.

The Moscow Times: Moscow Heat Breaks Another Record, The Moscow Times, 14th May, 2013.

Travis, K. R. and Jacob, D. J.: Systematic bias in evaluating chemical transport models with maximum daily 8 h average (MDA8) surface ozone for air quality applications: A case study with GEOS-Chem v9.02, Geosci Model Dev, 12, https://doi.org/10.5194/gmd-12-3641-2019, 2019.

Trigo, R. M., García-Herrera, R., Díaz, J., Trigo, I. F., and Valente, M. A.: How exceptional was the early August 2003 heatwave in France?, Geophys Res Lett, 32, https://doi.org/10.1029/2005GL022410, 2005.

Turnock, S. T., Allen, R. J., Andrews, M., Bauer, S. E., Deushi, M., Emmons, L., Good, P., Horowitz, L., John, J. G., Michou, M., Nabat, P., Naik, V., Neubauer, D., O'Connor, F. M., Olivié, D., Oshima, N., Schulz, M., Sellar, A., Shim, S., Takemura, T., Tilmes, S., Tsigaridis, K., Wu, T., and Zhang, J.: Historical and future changes in air pollutants from CMIP6 models, Atmos Chem Phys, 20, https://doi.org/10.5194/acp-20-14547-2020, 2020.

Turnock, S. T., Allen, R., Archibald, A. T., Dalvi, M., Folberth, G., Griffiths, P. T., Keeble, J., Robertson, E., and O'Connor, F. M.: The Future Climate and Air Quality Response

From Different Near-Term Climate Forcer, Climate, and Land-Use Scenarios Using UKESM1, Earths Future, 10, https://doi.org/10.1029/2022EF002687, 2022.

Vautard, R., Honoré, C., Beekmann, M., and Rouil, L.: Simulation of ozone during the August 2003 heat wave and emission control scenarios, Atmos Environ, 39, https://doi.org/10.1016/j.atmosenv.2005.01.039, 2005.

Vlachou, M., Brikas, D., and Pytharoulis, I.: Line - organised convection putting fire to forest area of Halkidiki, Northern Greece, in: 12th Plinius Conference on Mediterranean Storms, 84, 2010.

Willers, S. M., Jonker, M. F., Klok, L., Keuken, M. P., Odink, J., van den Elshout, S., Sabel, C. E., Mackenbach, J. P., and Burdorf, A.: High resolution exposure modelling of heat and air pollution and the impact on mortality, Environ Int, 89–90, https://doi.org/10.1016/j.envint.2016.01.013, 2016.

Yan, Y., Pozzer, A., Ojha, N., Lin, J., and Lelieveld, J.: Analysis of European ozone trends in the period 1995-2014, Atmos Chem Phys, 18, https://doi.org/10.5194/acp-18-5589-2018, 2018.

Yan, Y., Lin, J., Pozzer, A., Kong, S., and Lelieveld, J.: Trend reversal from high-to-low and from rural-to-urban ozone concentrations over Europe, Atmos Environ, 213, https://doi.org/10.1016/j.atmosenv.2019.05.067, 2019.

Young, P. J., Archibald, A. T., Bowman, K. W., Lamarque, J.-F., Naik, V., Stevenson, D. S., Tilmes, S., Voulgarakis, A., Wild, O., Bergmann, D., Cameron-Smith, P., Cionni, I., Collins, W. J., Dalsøren, S. B., Doherty, R. M., Eyring, V., Faluvegi, G., Horowitz, L. W., Josse, B., Lee, Y. H., MacKenzie, I. A., Nagashima, T., Plummer, D. A., Righi, M., Rumbold, S. T., Skeie, R. B., Shindell, D. T., Strode, S. A., Sudo, K., Szopa, S., and Zeng, G.: Pre-industrial to end 21st century projections of tropospheric ozone from the Atmospheric Chemistry and Climate Model Intercomparison Project (ACCMIP), Atmos Chem Phys, 13, https://doi.org/10.5194/acp-13-2063-2013, 2013.

Zanis, P., Akritidis, D., Turnock, S., Naik, V., Szopa, S., Georgoulias, A. K., Bauer, S. E., Deushi, M., Horowitz, L. W., Keeble, J., Le Sager, P., O'Connor, F. M., Oshima, N., Tsigaridis, K., and Van Noije, T.: Climate change penalty and benefit on surface ozone: A global perspective based on CMIP6 earth system models, Environmental Research Letters, 17, https://doi.org/10.1088/1748-9326/ac4a34, 2022.

Zohdirad, H., Jiang, J., Aksoyoglu, S., Namin, M. M., Ashrafi, K., and Prévôt, A. S. H.: Investigating sources of surface ozone in central Europe during the hot summer in 2018: High temperatures, but not so high ozone, Atmos Environ, 279, https://doi.org/10.1016/j.atmosenv.2022.119099, 2022.

Table S1: *Ten largest ozone episodes according to their areal extent over [10° W-50° E; 34°-60° N] in CAMS during April-September 2003-2022. Columns indicate (from left to right) the start date, duration, and areal extent of each episode.*

Start date	Duration (days)	Areal extent (10^4 km^2)
2-8-2003	18	4551
21-7-2010	30	3972
13-7-2006	18	3044
18-9-2003	10	1855
29-6-2003	11	1483
12-8-2006	9	1368
20-7-2007	7	1241
7-5-2013	6	1117
28-4-2006	11	1071
19-7-2003	8	1041

Figure 1

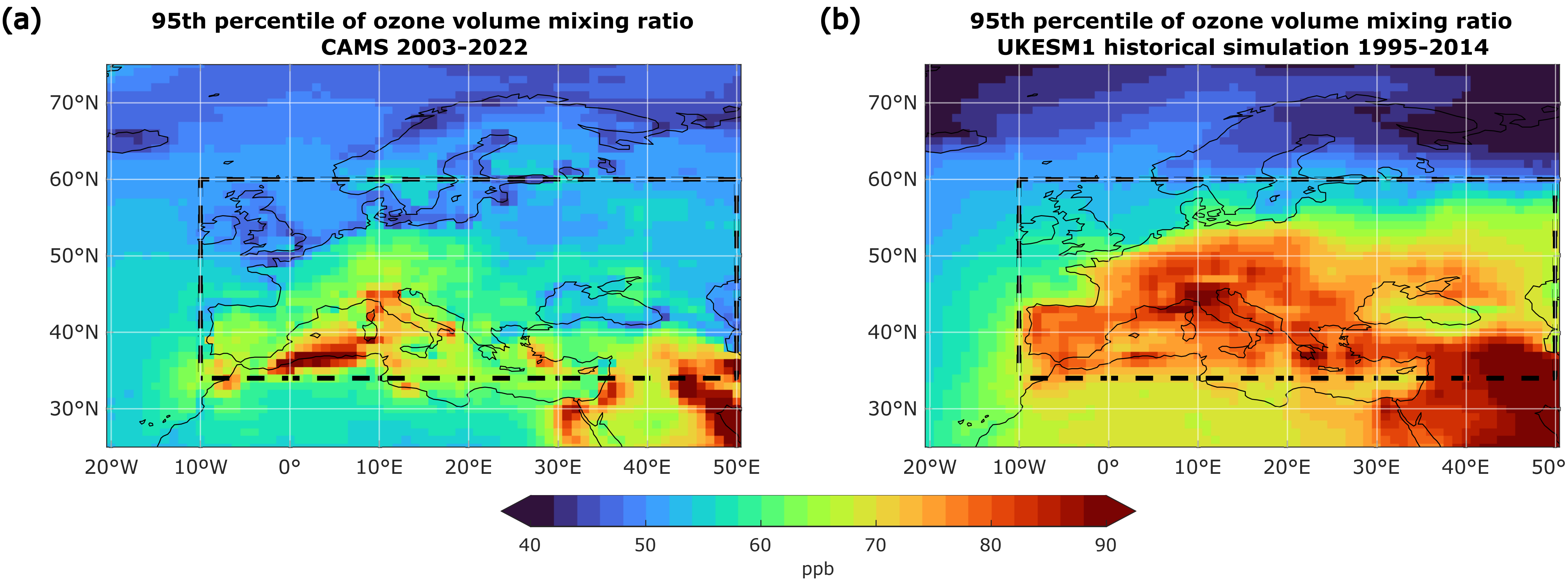
(a)
95th percentile of ozone volume mixing ratio
CAMS 2003-2022
(b)
95th percentile of ozone volume mixing ratio
UKESM1 historical simulation 1995-2014
70°N
60°N
50°N
40°N
30°N
20°W
10°W
0°
10°E
20°E
30°E
40°E
50°E
40
50
60
70
80
90
ppb

Figure 2

Click here to access/download;Figure;Fig2.eps

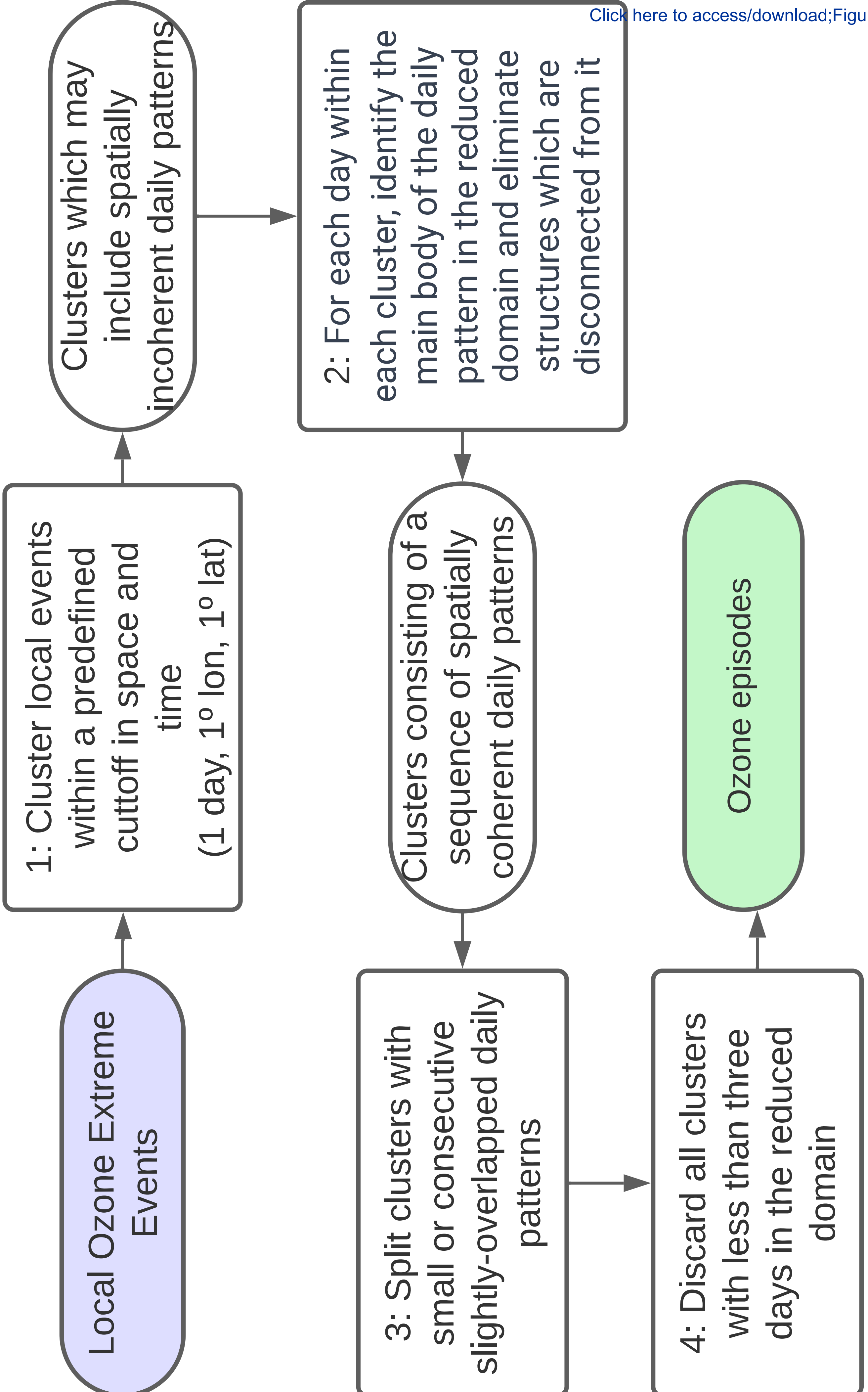

Figure 3

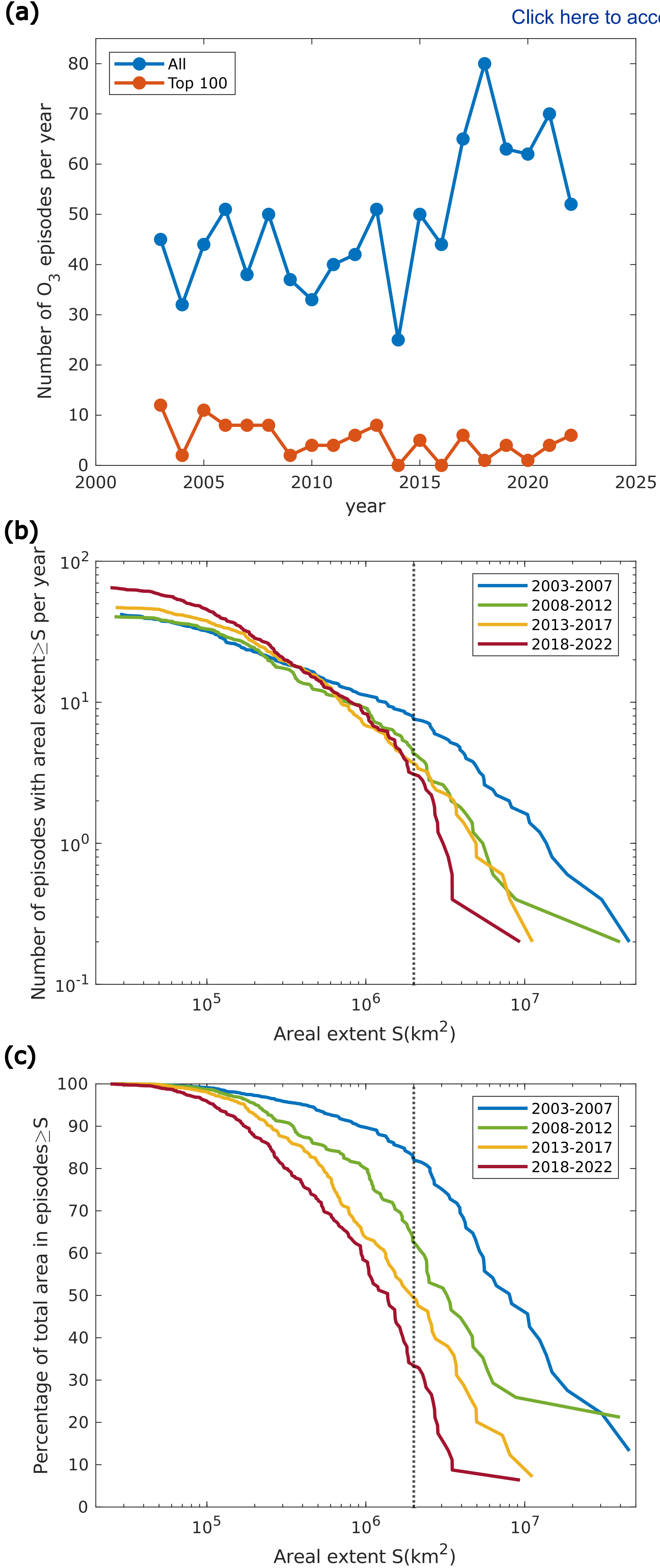
(a)
All
Top 100
Number of O_3 episodes per year
year
(b)
2003-2007
2008-2012
2013-2017
2018-2022
Number of episodes with areal extent≥S per year
Areal extent S(km^2)
(c)
2003-2007
2008-2012
2013-2017
2018-2022
Percentage of total area in episodes≥S
Areal extent S(km^2)

Figure 4

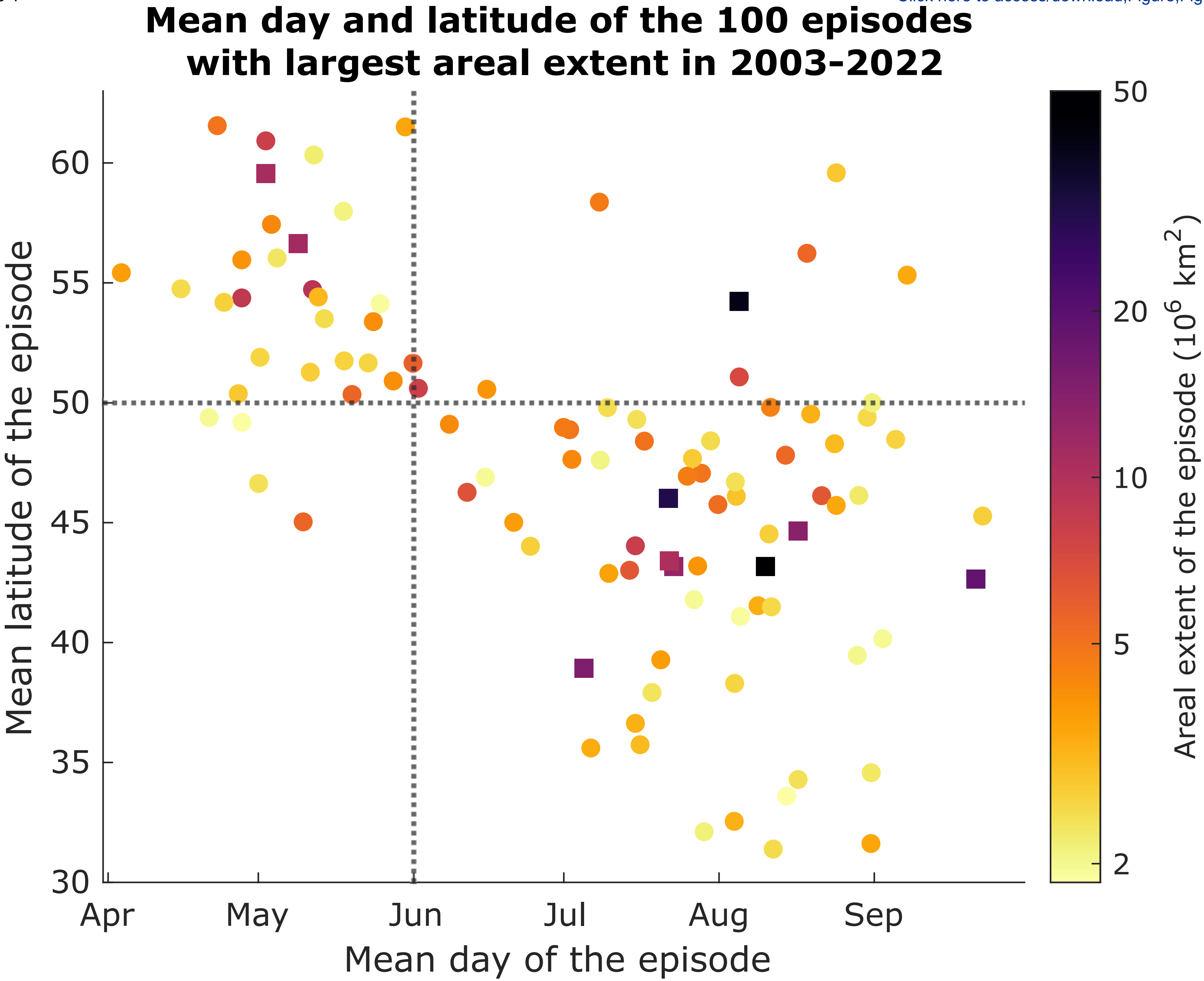
Mean day and latitude of the 100 episodes
with largest areal extent in 2003-2022
Mean latitude of the episode
60
55
50
45
40
35
30
Apr
May
Jun
Jul
Aug
Sep
Mean day of the episode
Areal extent of the episode (10^6 km^2)
50
20
10
5
2

Figure 5

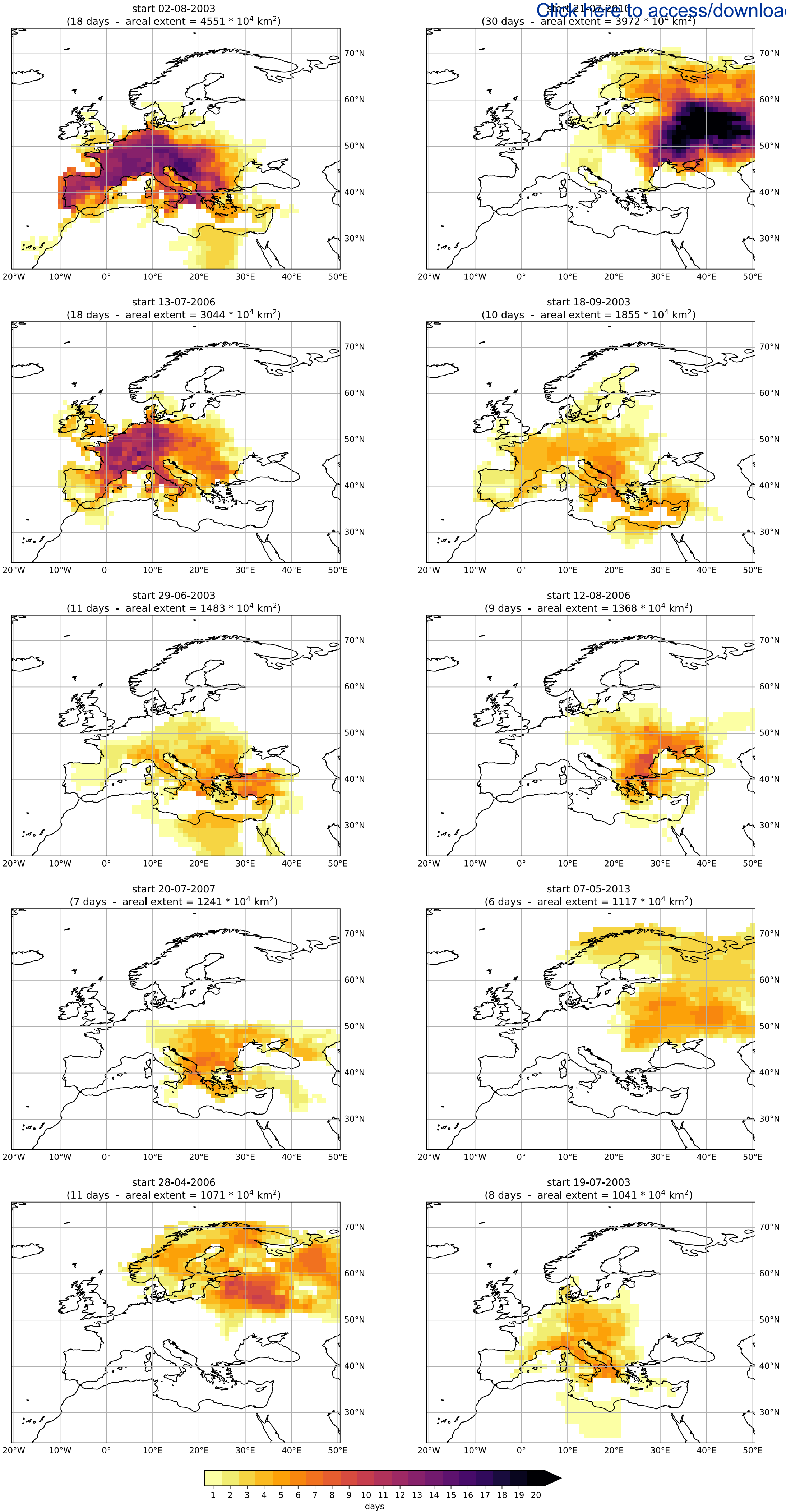
start 02-08-2003
(18 days - areal extent = 4551 * 10^4 km^2)
(30 days - areal extent = 3972 * 10^4 km^2)
start 13-07-2006
(18 days - areal extent = 3044 * 10^4 km^2)
start 18-09-2003
(10 days - areal extent = 1855 * 10^4 km^2)
start 29-06-2003
(11 days - areal extent = 1483 * 10^4 km^2)
start 12-08-2006
(9 days - areal extent = 1368 * 10^4 km^2)
start 20-07-2007
(7 days - areal extent = 1241 * 10^4 km^2)
start 07-05-2013
(6 days - areal extent = 1117 * 10^4 km^2)
start 28-04-2006
(11 days - areal extent = 1071 * 10^4 km^2)
start 19-07-2003
(8 days - areal extent = 1041 * 10^4 km^2)
20°W 10°W 0° 10°E 20°E 30°E 40°E 50°E
30°N 40°N 50°N 60°N 70°N
1 2 3 4 5 6 7 8 9 10 11 12 13 14 15 16 17 18 19 20
days

Figure 6

Click here to access/download;Figure;Fig6.eps

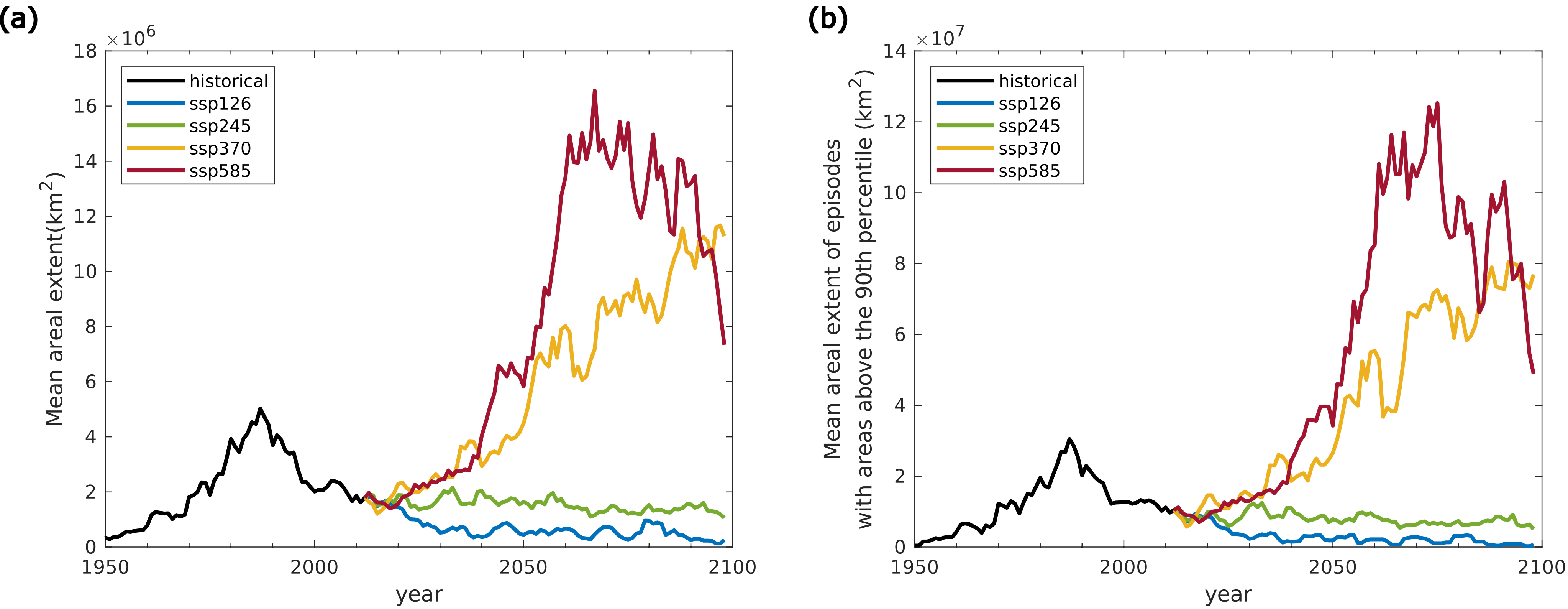

Figure 7

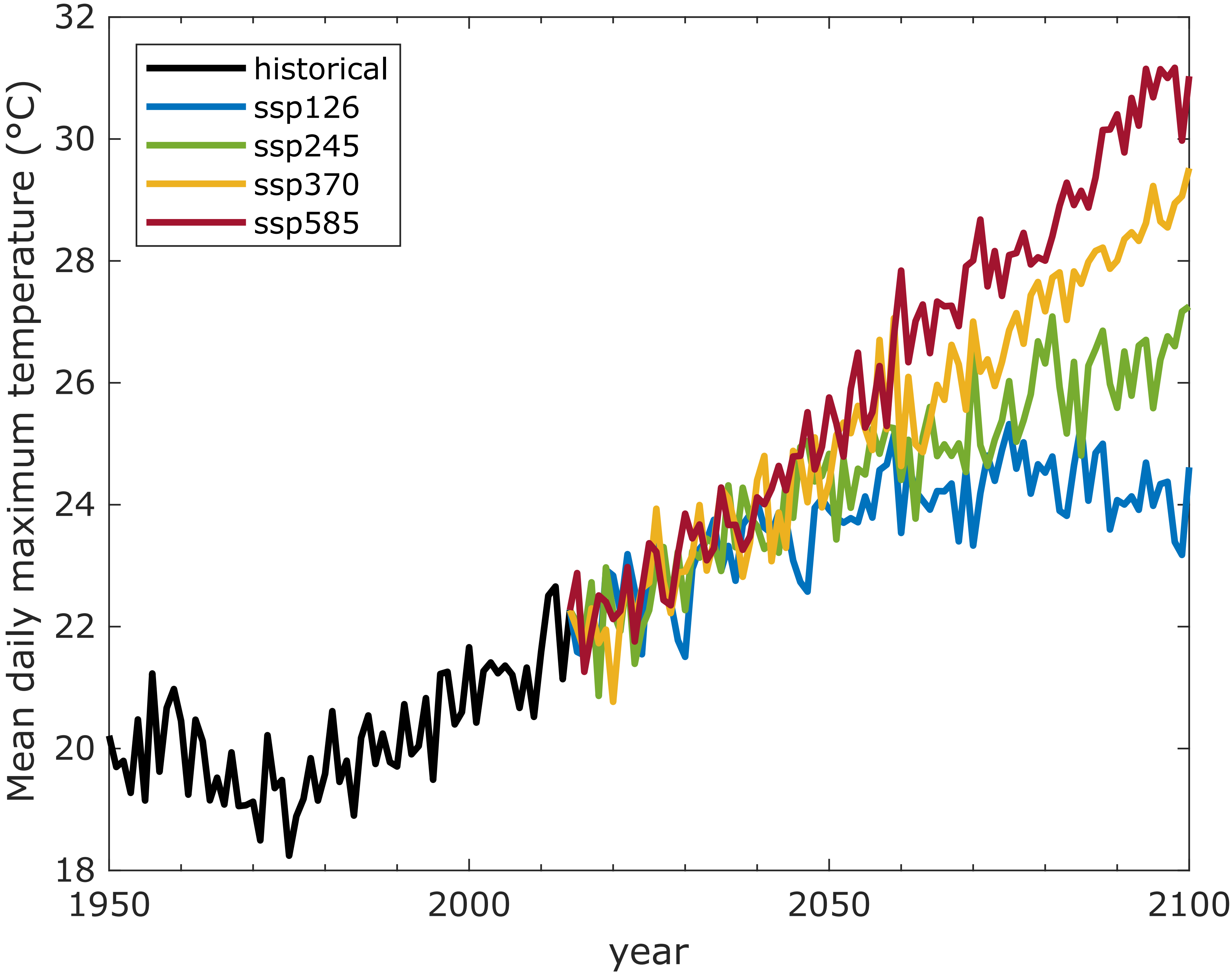
historical
ssp126
ssp245
ssp370
ssp585
Mean daily maximum temperature (°C)
32
30
28
26
24
22
20
18
1950
2000
2050
2100
year

Figure 8

Click here to access/download;Figure;Fig8.eps

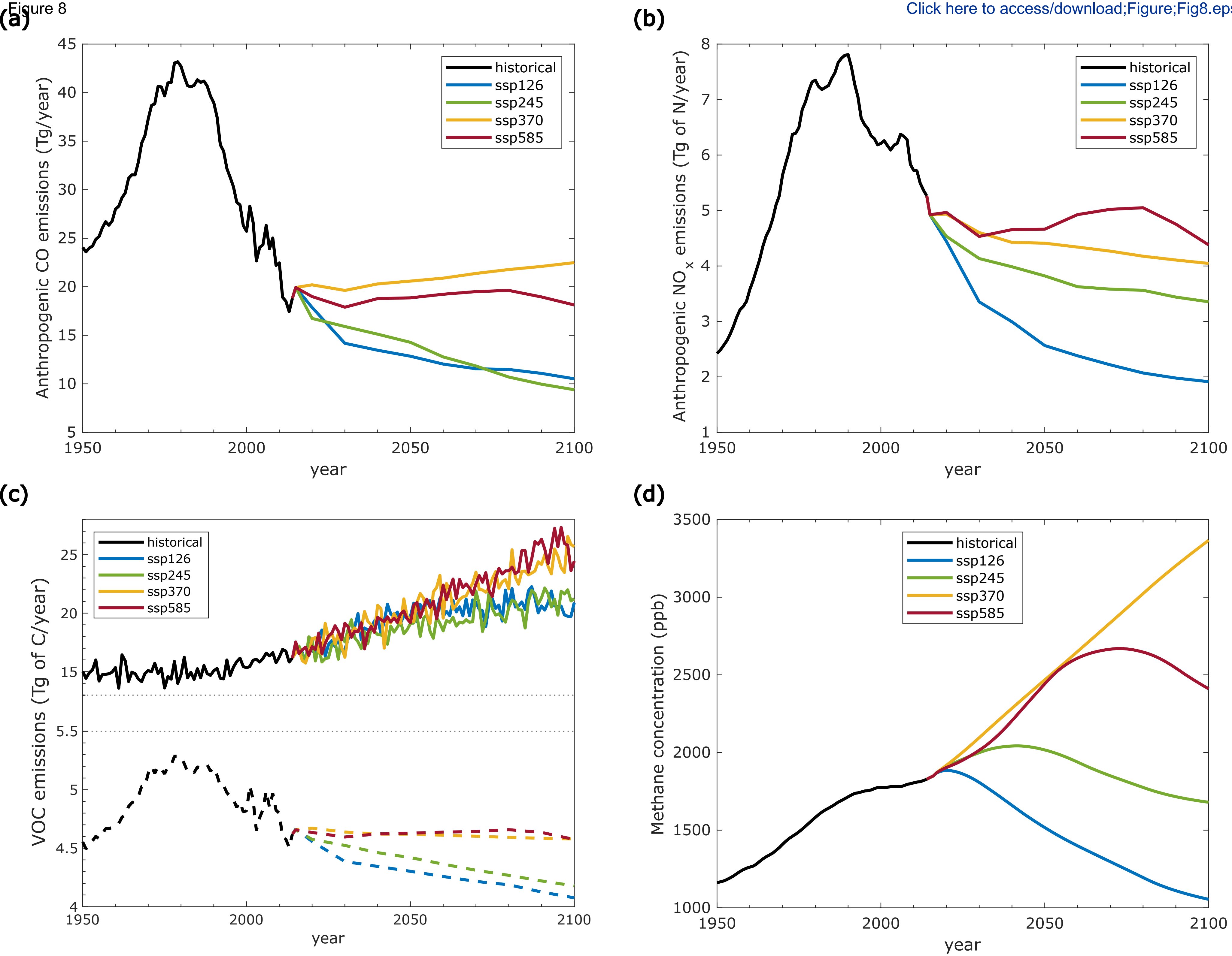

Figure S1

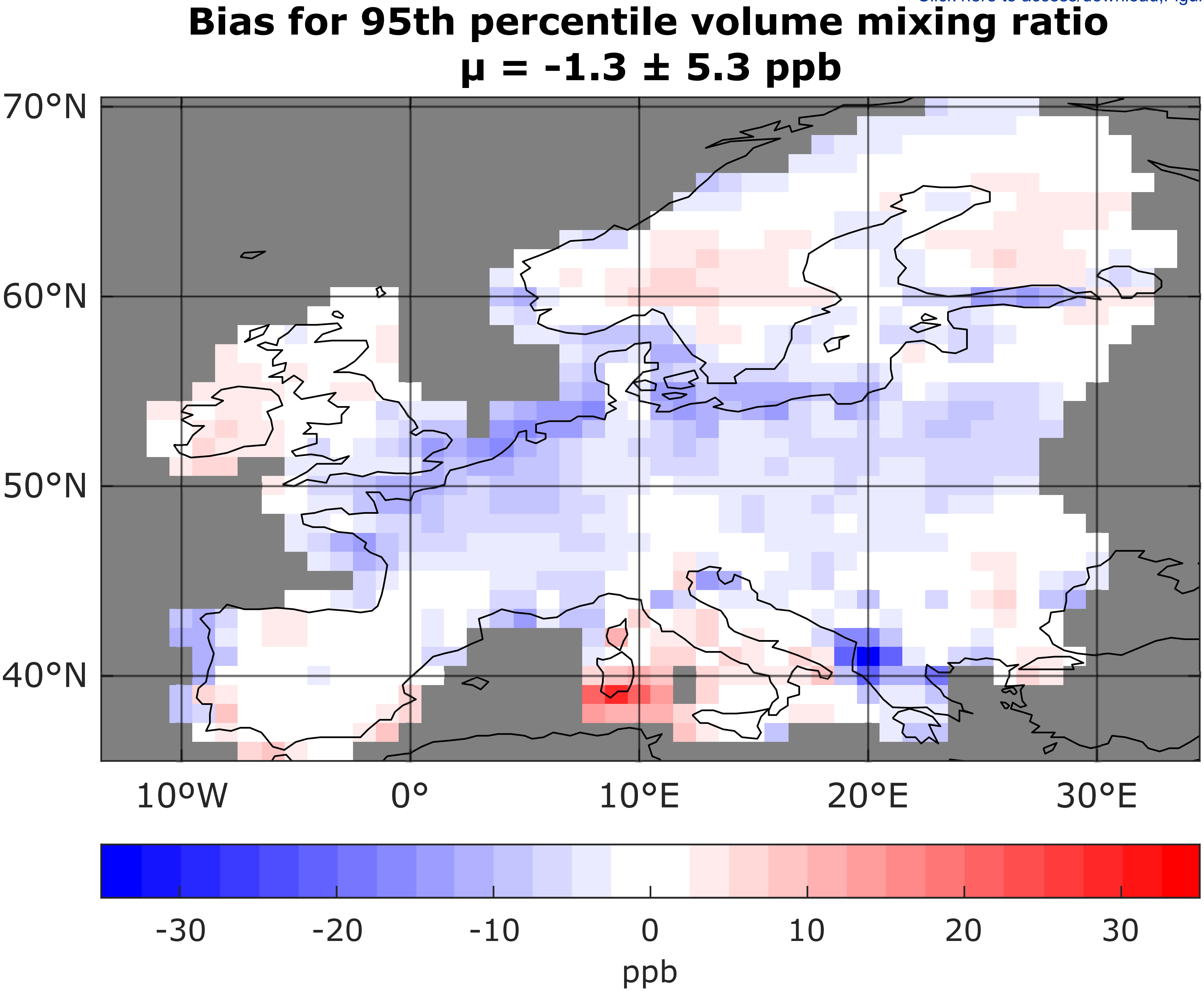
Bias for 95th percentile volume mixing ratio
μ = -1.3 ± 5.3 ppb
70°N
60°N
50°N
40°N
10°W
0°
10°E
20°E
30°E
-30
-20
-10
0
10
20
30
ppb

Figure S2

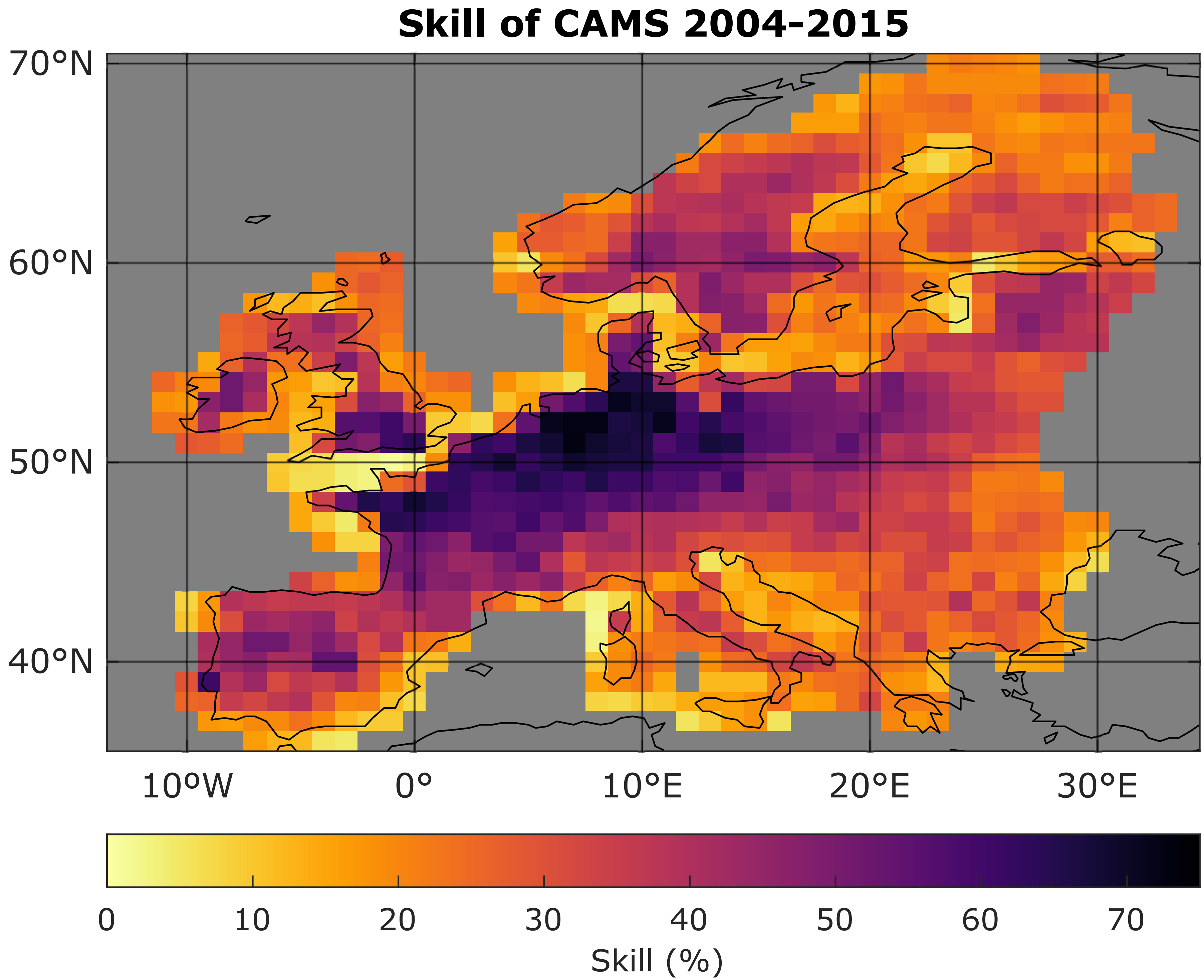
Skill of CAMS 2004-2015
70°N
60°N
50°N
40°N
10°W
0°
10°E
20°E
30°E
0
10
20
30
40
50
60
70
Skill (%)

Figure S3

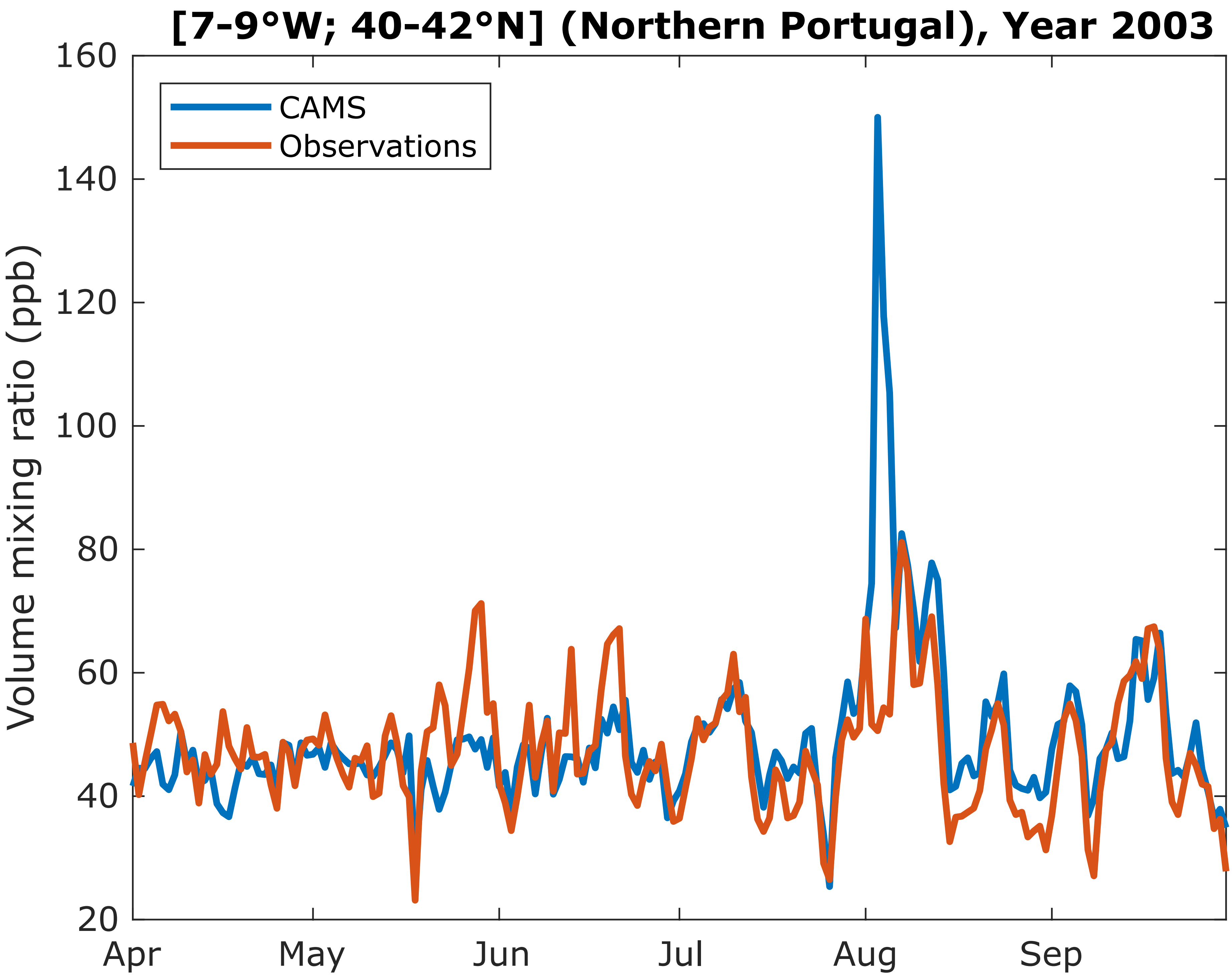
[7-9°W; 40-42°N] (Northern Portugal), Year 2003
CAMS
Observations
Volume mixing ratio (ppb)
160
140
120
100
80
60
40
20
Apr
May
Jun
Jul
Aug
Sep

Figure S4

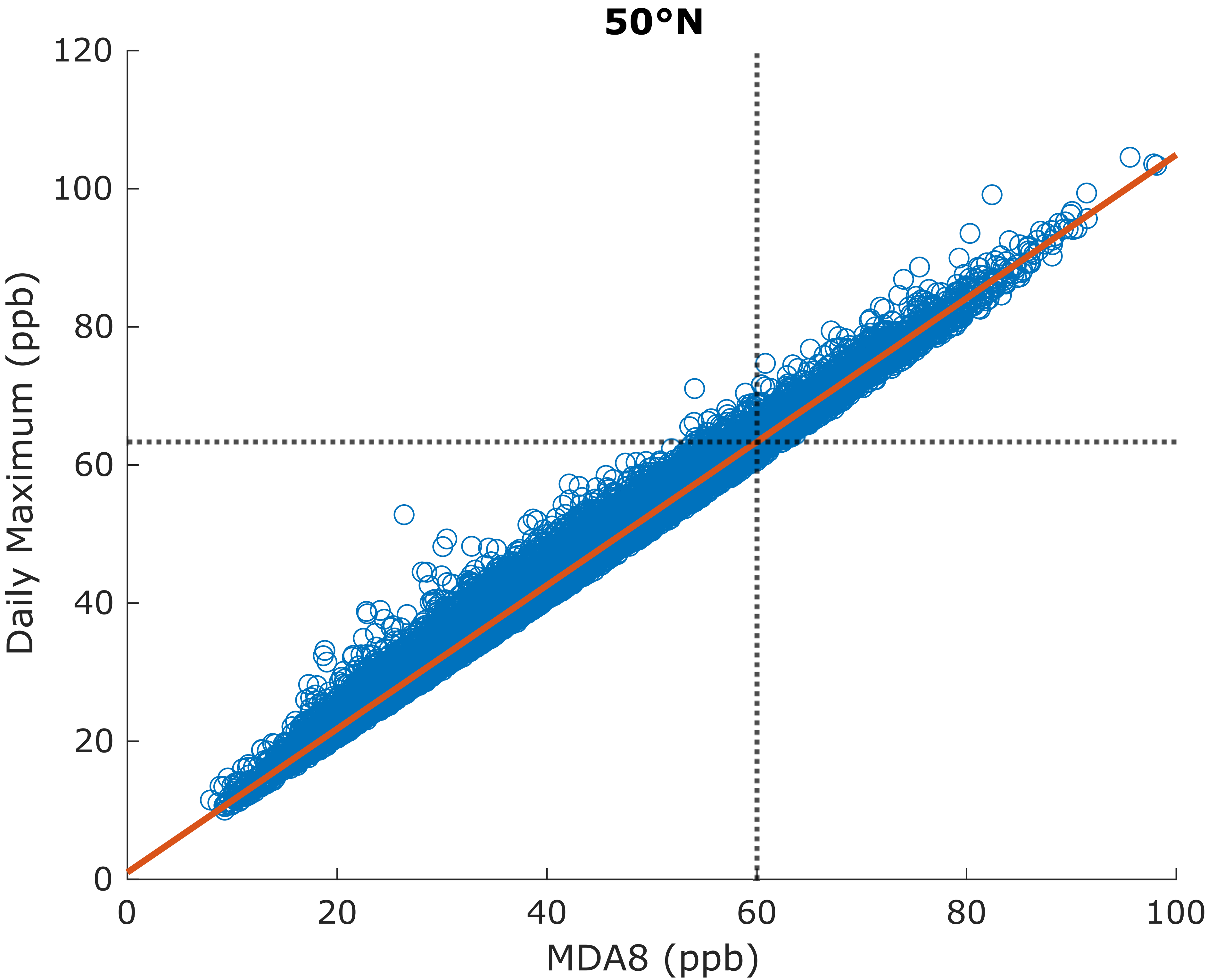
50°N
120
100
80
60
40
20
0
Daily Maximum (ppb)
0
20
40
60
80
100
MDA8 (ppb)

Figure S5

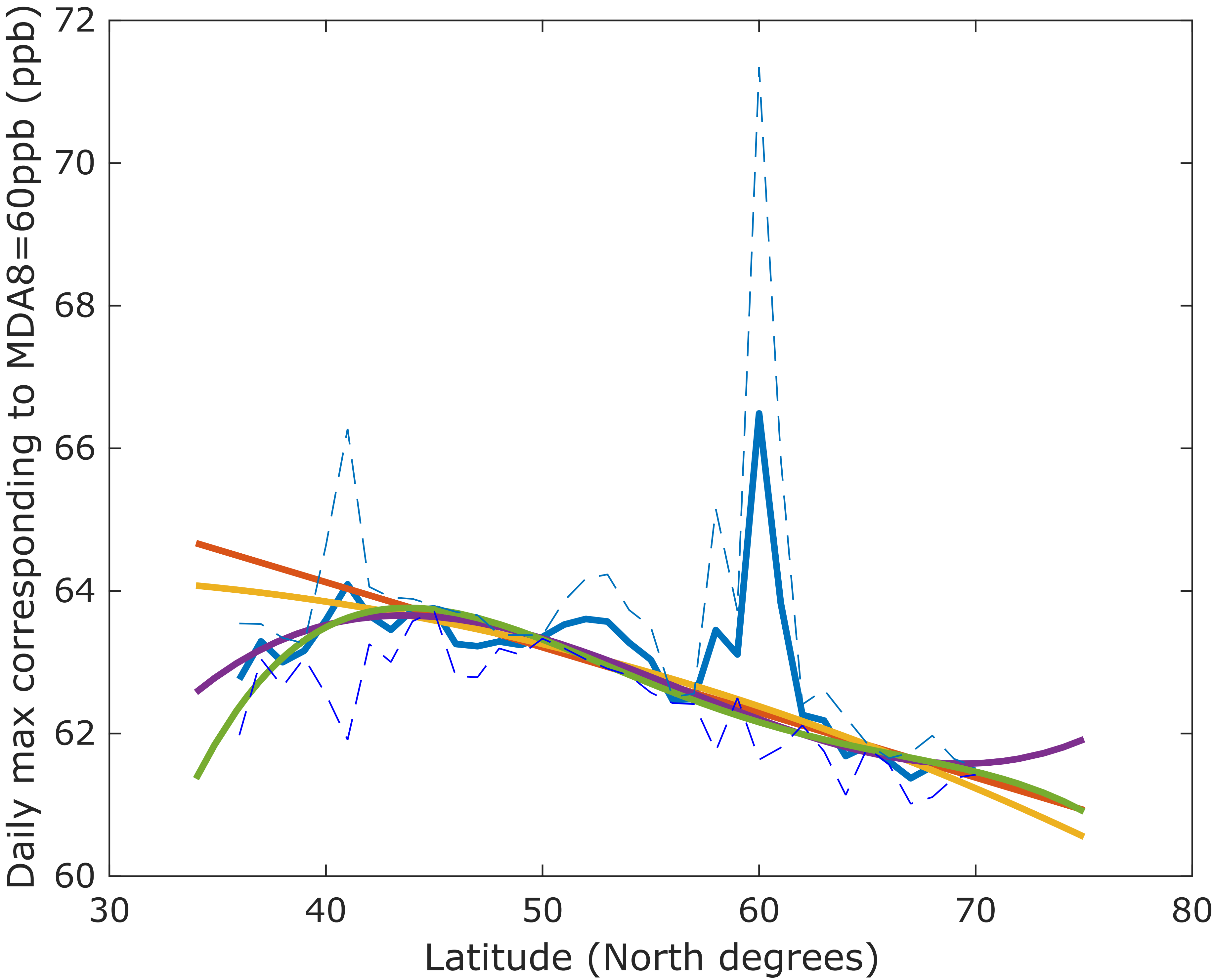
Daily max corresponding to MDA8=60ppb (ppb)
Latitude (North degrees)
72
70
68
66
64
62
60
30
40
50
60
70
80

Figure S6

Click here to access/download;Figure;FigS6.eps

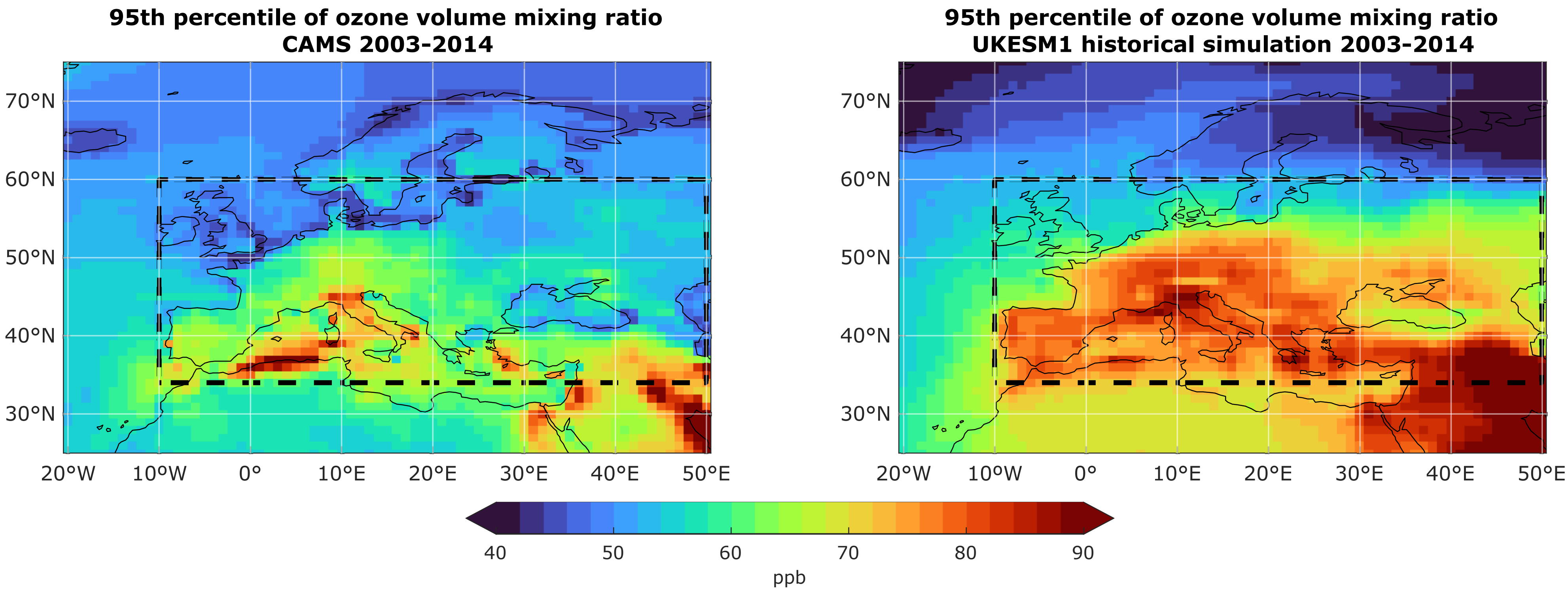

Figure S7

Click here to access/download;Figure;FigS7.eps

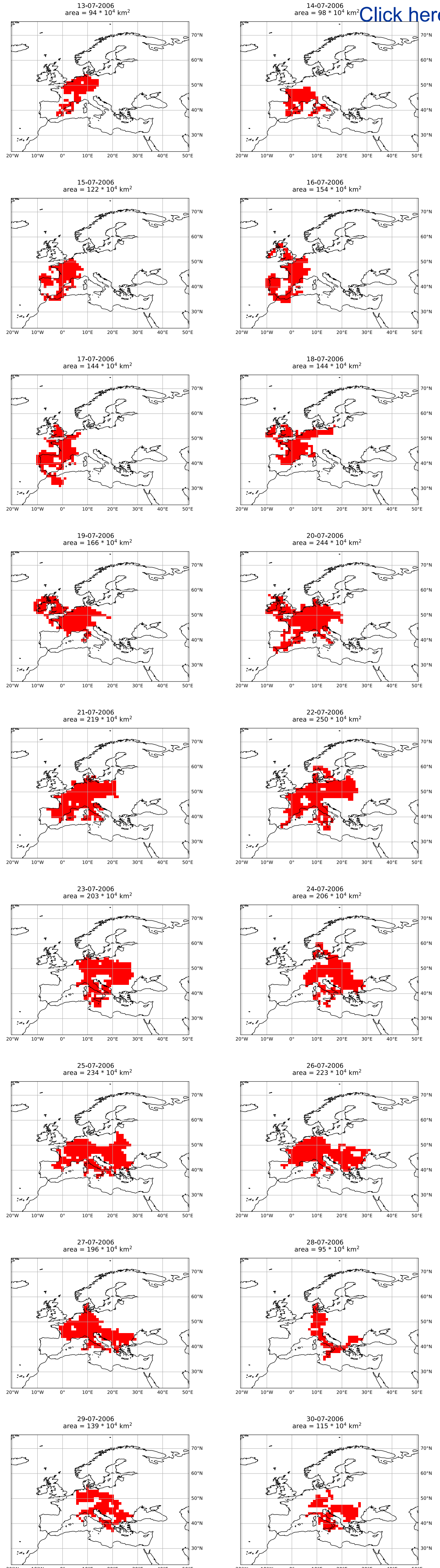

Figure S8

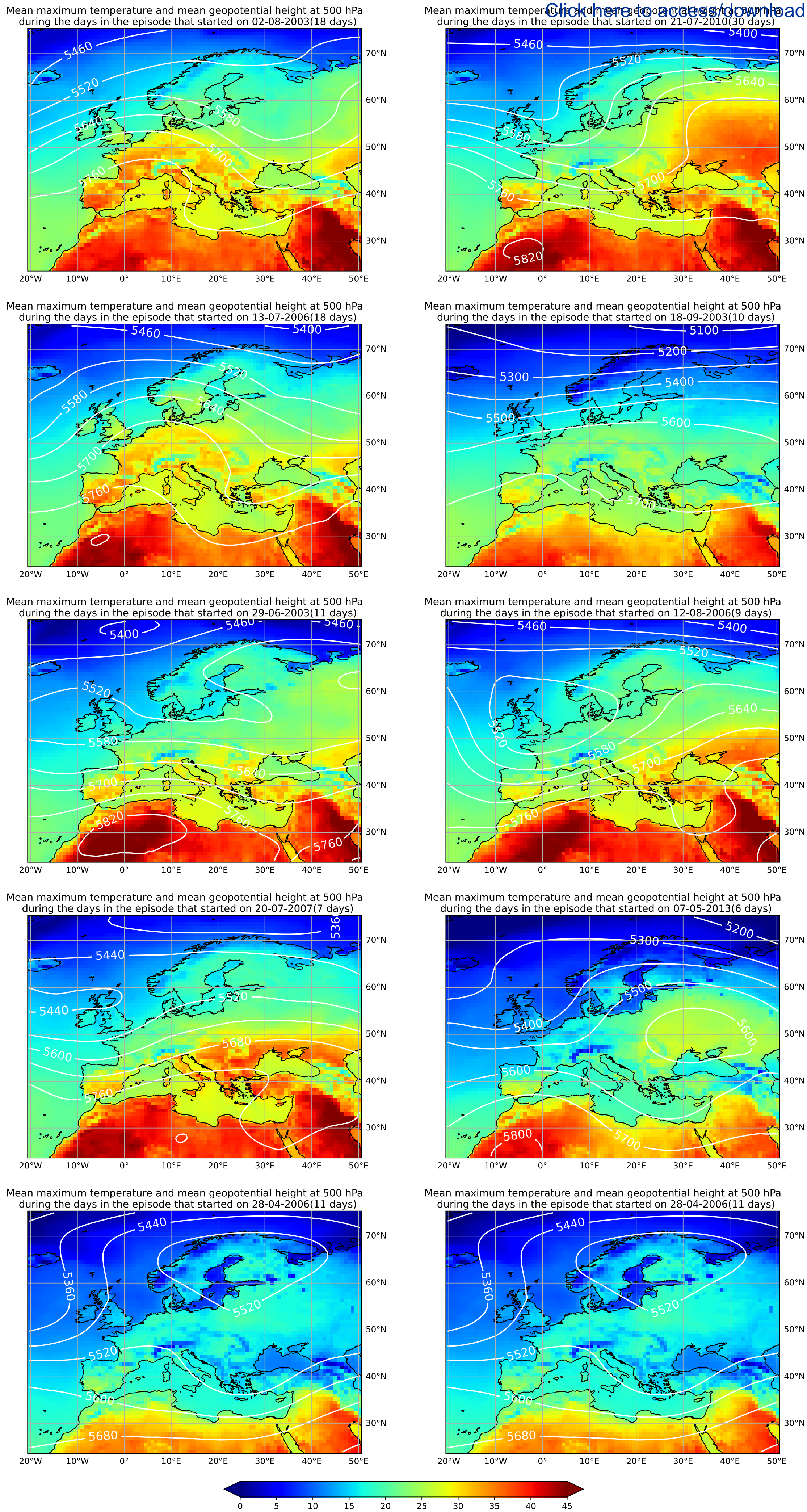
Mean maximum temperature and mean geopotential height at 500 hPa during the days in the episode that started on 02-08-2003(18 days)
Mean maximum temperature and mean geopotential height at 500 hPa during the days in the episode that started on 21-07-2010(30 days)
Mean maximum temperature and mean geopotential height at 500 hPa during the days in the episode that started on 13-07-2006(18 days)
Mean maximum temperature and mean geopotential height at 500 hPa during the days in the episode that started on 18-09-2003(10 days)
Mean maximum temperature and mean geopotential height at 500 hPa during the days in the episode that started on 29-06-2003(11 days)
Mean maximum temperature and mean geopotential height at 500 hPa during the days in the episode that started on 12-08-2006(9 days)
Mean maximum temperature and mean geopotential height at 500 hPa during the days in the episode that started on 20-07-2007(7 days)
Mean maximum temperature and mean geopotential height at 500 hPa during the days in the episode that started on 07-05-2013(6 days)
Mean maximum temperature and mean geopotential height at 500 hPa during the days in the episode that started on 28-04-2006(11 days)
Mean maximum temperature and mean geopotential height at 500 hPa during the days in the episode that started on 28-04-2006(11 days)
20°W 10°W 0° 10°E 20°E 30°E 40°E 50°E
30°N 40°N 50°N 60°N 70°N
0 5 10 15 20 25 30 35 40 45
°C

Figure S9

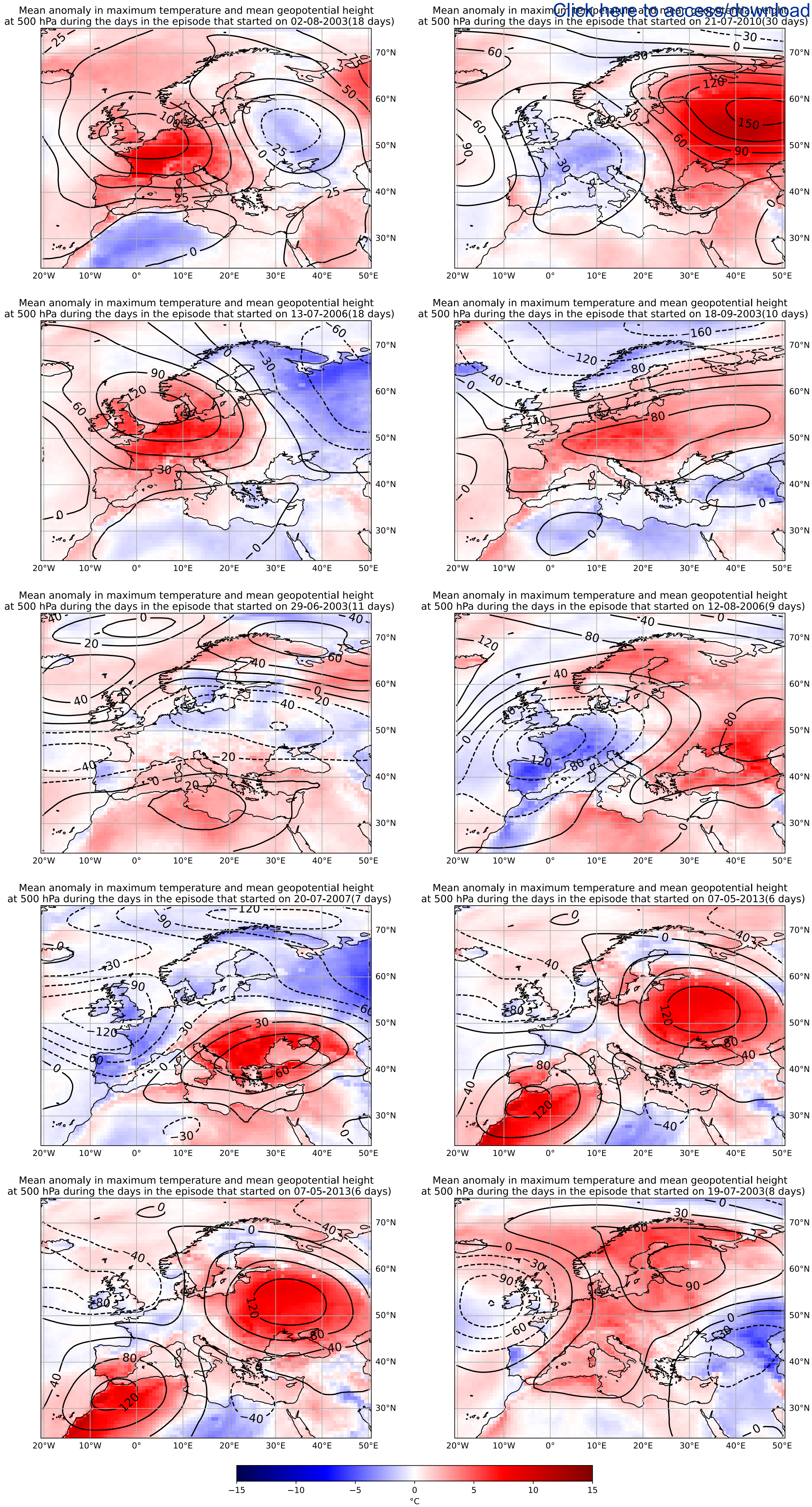
Mean anomaly in maximum temperature and mean geopotential height at 500 hPa during the days in the episode that started on 02-08-2003(18 days)
Mean anomaly in maximum temperature and mean geopotential height at 500 hPa during the days in the episode that started on 21-07-2010(30 days)
Mean anomaly in maximum temperature and mean geopotential height at 500 hPa during the days in the episode that started on 13-07-2006(18 days)
Mean anomaly in maximum temperature and mean geopotential height at 500 hPa during the days in the episode that started on 18-09-2003(10 days)
Mean anomaly in maximum temperature and mean geopotential height at 500 hPa during the days in the episode that started on 29-06-2003(11 days)
Mean anomaly in maximum temperature and mean geopotential height at 500 hPa during the days in the episode that started on 12-08-2006(9 days)
Mean anomaly in maximum temperature and mean geopotential height at 500 hPa during the days in the episode that started on 20-07-2007(7 days)
Mean anomaly in maximum temperature and mean geopotential height at 500 hPa during the days in the episode that started on 07-05-2013(6 days)
Mean anomaly in maximum temperature and mean geopotential height at 500 hPa during the days in the episode that started on 07-05-2013(6 days)
Mean anomaly in maximum temperature and mean geopotential height at 500 hPa during the days in the episode that started on 19-07-2003(8 days)
20°W 10°W 0° 10°E 20°E 30°E 40°E 50°E
30°N 40°N 50°N 60°N 70°N
−15 −10 −5 0 5 10 15
°C

Figure S10

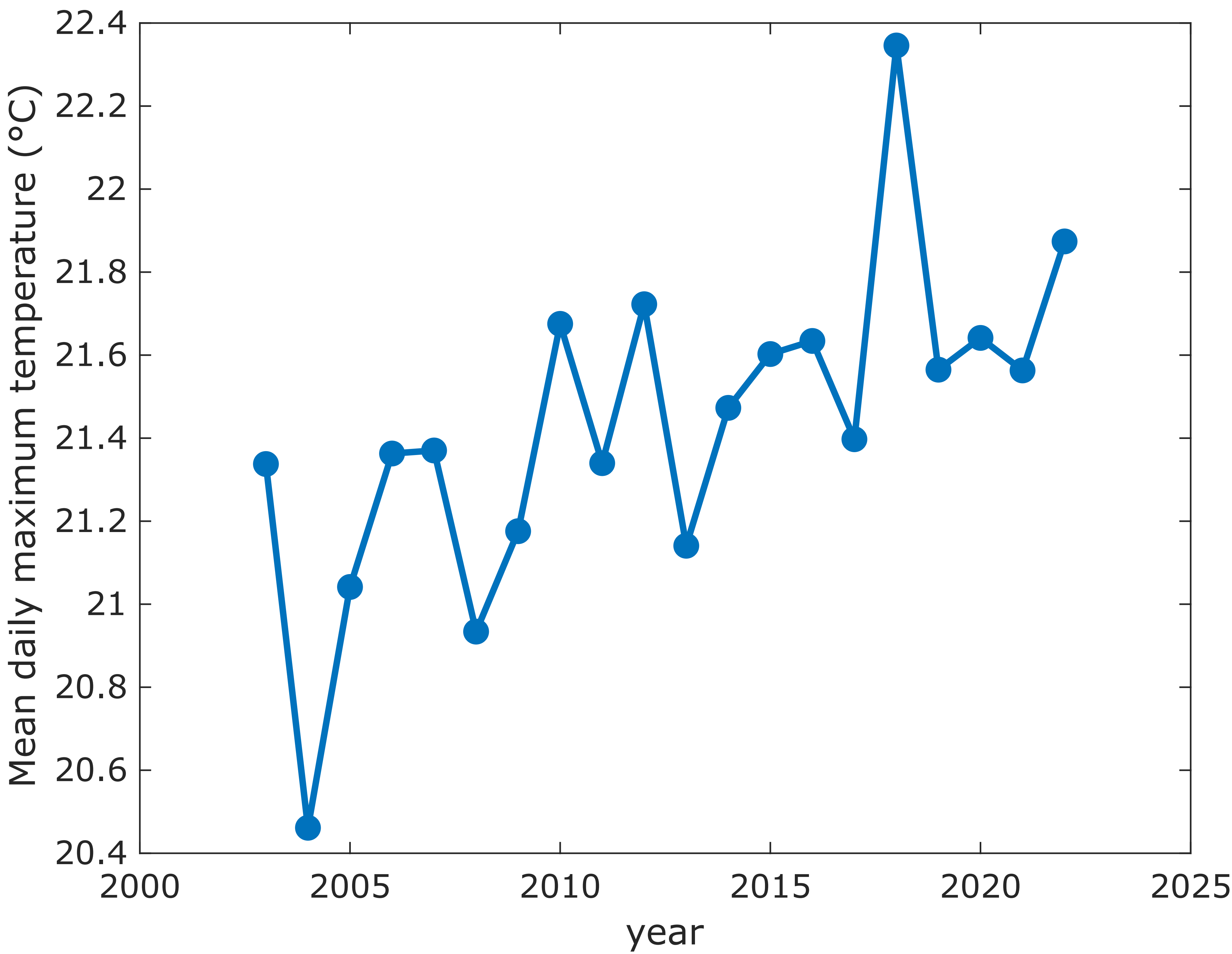
22.4
22.2
22
21.8
21.6
21.4
21.2
21
20.8
20.6
20.4
Mean daily maximum temperature (°C)
2000
2005
2010
2015
2020
2025
year

Figure S11

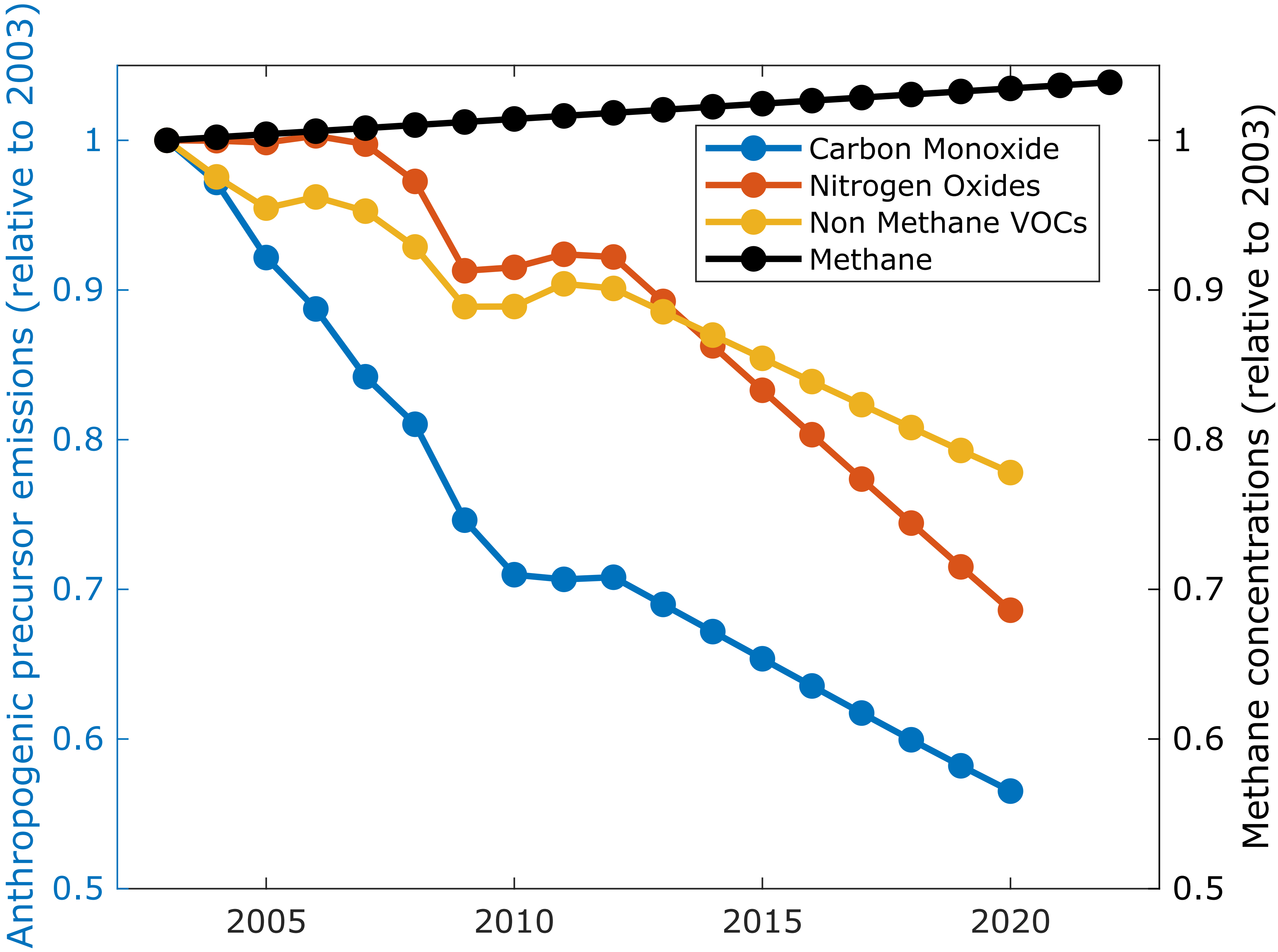
Anthropogenic precursor emissions (relative to 2003)
1
0.9
0.8
0.7
0.6
0.5
2005
2010
2015
2020
year
Methane concentrations (relative to 2003)
Carbon Monoxide
Nitrogen Oxides
Non Methane VOCs
Methane

Figure S12

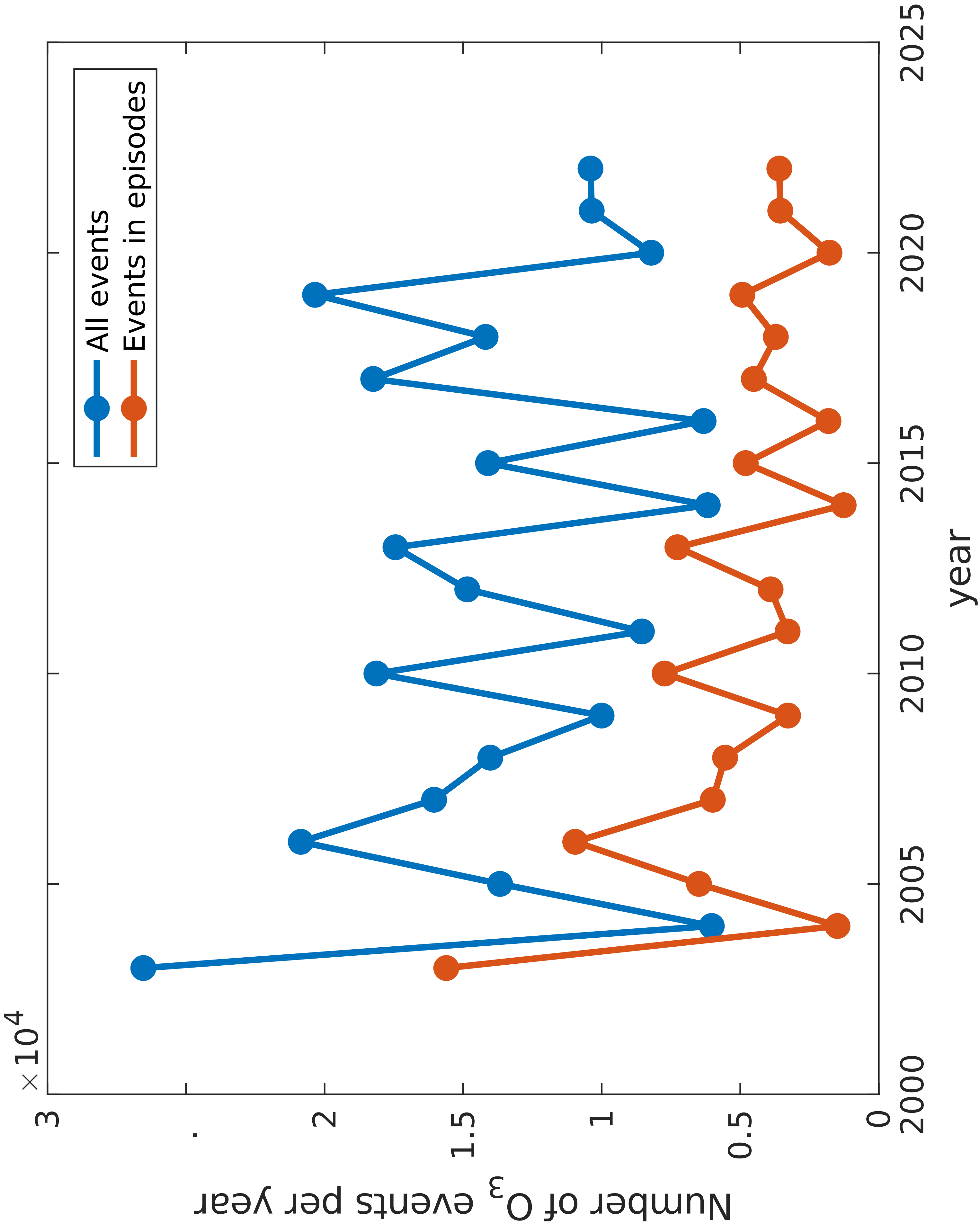
All events
Events in episodes
year
Number of O_3 events per year
$\times 10^4$
2000
2005
2010
2015
2020
2025
0
0.5
1
1.5
2
3

Figure S13

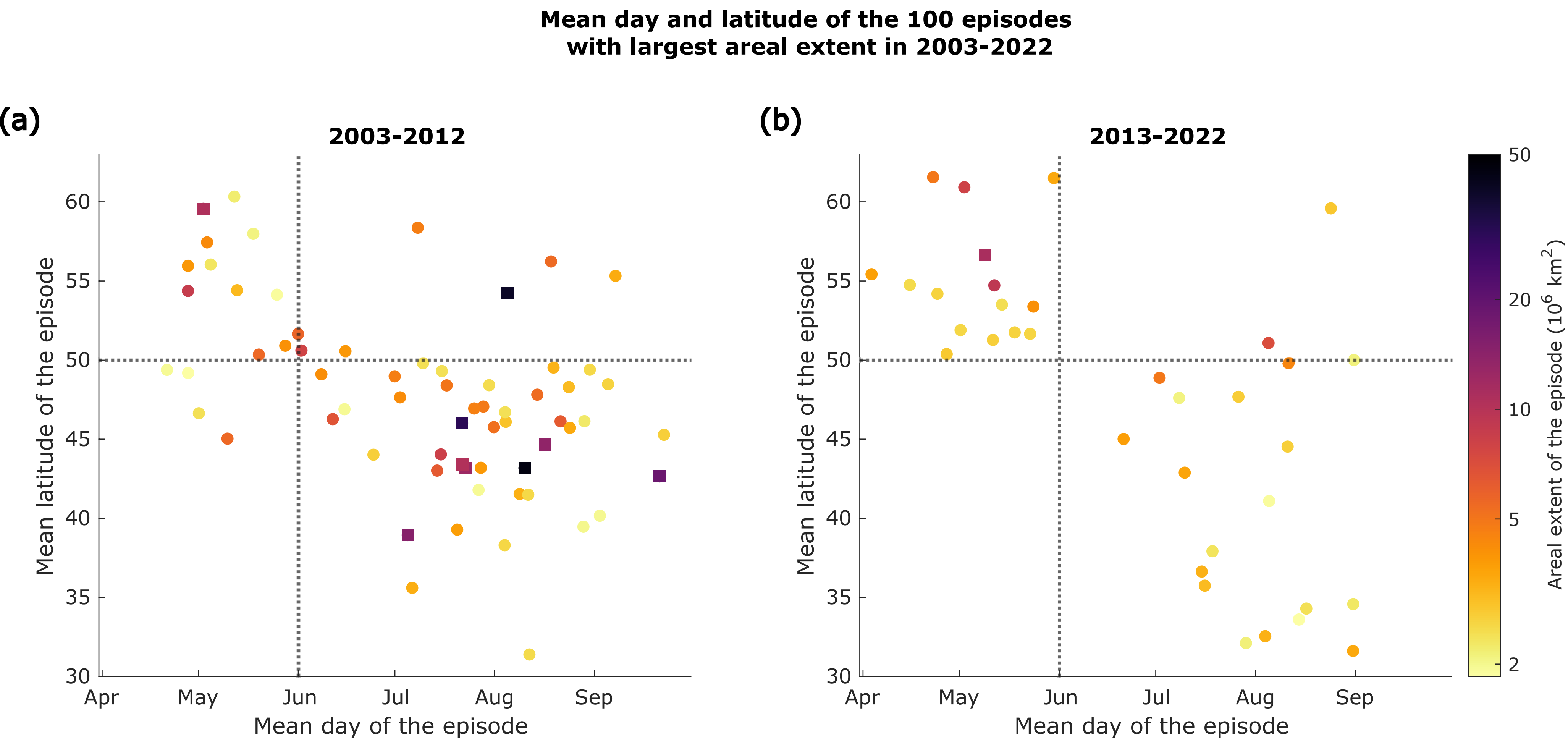
Mean day and latitude of the 100 episodes
with largest areal extent in 2003-2022
(a)
2003-2012
(b)
2013-2022
Mean latitude of the episode
60
55
50
45
40
35
30
Apr
May
Jun
Jul
Aug
Sep
Mean day of the episode
Areal extent of the episode (10^6 km^2)
50
20
10
5
2